

Bayesian Solution Uncertainty Quantification for Differential Equations

Oksana A. Chkrebtii*, David A. Campbell†, Ben Calderhead‡, Mark A. Girolami§

October 12, 2021

Abstract

We explore the use of probability models for uncertainty arising from discretization of system states defined implicitly by ordinary or partial differential equations. Accounting for this uncertainty is vital for characterising potential inferential bias incurred when likelihoods are constructed based on a numerical approximation over a finite discretization grid. A formalism for inferring fixed but a priori unknown model trajectories is proposed within the forward problem through Bayesian updating of sequentially refined prior models conditional on model interrogations. A one-step-ahead sampling scheme for interrogating the model is studied in detail, its consistency and first order convergence properties are proved. The proposed approach is demonstrated to capture the functional structure and magnitude of the discretization error, while attaining computational scaling of the same order as traditional first order numerical methods, and providing a formal statistical trade-off between accuracy and discretization grid size. Examples illustrate the flexibility of this framework to deal with a wide variety of models that include initial value, delay, and boundary value ordinary differential equations, as well as partial differential equations. Scalability is illustrated for a model of fluid dynamics consisting of over 16,000 coupled, stiff ordinary differential equations. Within the inverse problem, discretization uncertainty is defined as an additional layer in the Bayesian hierarchy, and a Markov chain Monte Carlo sampling scheme that targets the resulting posterior distribution is developed. This formalism is used to infer states and parameters for the JAK-STAT delay differential equation network of protein dynamics from indirectly observed measurements. Finally, the discussion outlines a wide range of emerging research themes in the new field of probabilistic numerics that naturally follow from the work presented.

Keywords: Bayesian Numerical Analysis, Uncertainty Quantification, Gaussian Processes, Differential Equation Models, Uncertainty in Computer Models.

1 Quantifying Uncertainty for Differential Equation Models

Many scientific, economic, and engineering disciplines represent the spatio-temporal evolution of complex systems implicitly as differential equations, using few but readily interpretable parameters, $\theta \in \Theta$. Partial differential equation (PDE) models describe the natural dependence between system states, $u : \mathcal{D} \times \Theta \rightarrow \mathbb{R}^P$, and their rates of change over the spatio-temporal domain $\mathcal{D} = \mathcal{X} \times \mathcal{T}$ through a given function F . Model states, u , are specified implicitly as those satisfying the equation,

$$F\left(x, t, \frac{\partial u}{\partial t}, \frac{\partial u}{\partial x_1}, \frac{\partial u}{\partial x_2}, \frac{\partial^2 u}{\partial x_1 \partial x_2}, \dots, u, \theta\right) = 0, \quad x \in \mathcal{X}, t \in \mathcal{T},$$

with additional constraints, usually given at the boundary of \mathcal{D} . When states evolve solely with respect to a single variable, such as time, the model is reduced to the ordinary differential equation (ODE),

$$\frac{du}{dt} = f(t, u, \theta), \quad t \in \mathcal{T},$$

*Department of Statistics, The Ohio State University, Columbus, OH 43210-1247, USA; oksana@stat.osu.edu

†Department of Statistics and Actuarial Science, Simon Fraser University, Burnaby, BC, V5A 1S6 Canada

‡Department of Mathematics, Imperial College London, London SW7 2AZ, UK

§Department of Statistics, The University of Warwick, Coventry CV4 7AL, UK

with associated constraints at the boundary of \mathcal{T} . The explicit solution of a differential equation model at evaluation points $(\mathbf{x}, \mathbf{t}) \in \mathcal{D}^T$, represented by $u^*(\mathbf{x}, \mathbf{t}, \theta)$, is used to explore system dynamics, design experiments, or extrapolate to expensive or dangerous circumstances. Therefore, increasing attention is being paid to the challenges associated with quantifying uncertainty for systems defined by differential equations, and in particular those based on mathematical descriptions of complex phenomena such as the weather, ocean currents, ice sheet flow, and cellular protein transport (Ghanem and Spanos, 2003; Huttunen and Kaipio, 2007; Kaipio et al., 2004; Marzouk and Najm, 2009; Marzouk et al., 2007; Stuart, 2010).

The main challenge of working with differential equation models, from both mathematical and statistical perspectives, is that solutions are generally not available in closed form. When this occurs, prior exploration of the mathematical model, $u^*(\mathbf{x}, \mathbf{t}, \theta)$, cannot be performed directly. This issue is dealt with throughout the literature by replacing the exact solution with an N -dimensional approximate solution, $\hat{u}^N(\mathbf{x}, \mathbf{t}, \theta)$, obtained using numerical techniques over a size N partition of the domain \mathcal{D} . Inference and prediction based on $\hat{u}^N(\mathbf{x}, \mathbf{t}, \theta)$ then inform the reasoning process when, for example, assessing financial risk in deciding on oil field bore configurations, or forming government policy in response to extreme weather events.

Because such systems are often highly nonlinear, the seemingly innocuous assumption of negligible numerical error can lead to serious model bias. Limited computation and coarse mesh size are contributors to numerical error, as described in the comprehensive overview of Oberkampf and Roy (2010). For complex, large-scale models, maintaining a mesh size that is fine enough to ignore discretization uncertainty often demands prohibitive computational cost (Arridge et al., 2006), so that a coarse mesh is often the only feasible choice despite associated model uncertainty (Kim et al., 2014).

The study of how uncertainty propagates through a mathematical model is known as the *forward problem*. Various aspects of this problem have been investigated in the engineering and applied mathematics literature, but few have considered uncertainty arising from model approximation from a statistical perspective. Numerical error analysis provides local and global discretization error bounds that are characterized point-wise and relate to the asymptotic behaviour of the deterministic approximation of the model. However, accounting for this type of *verification error* for the purpose of model inference has proven to be a difficult open problem (Oberkampf and Roy, 2010), causing discretization uncertainty to be often ignored in practice.

Indeed, in the many cases where discretization error is not negligible, for example in large scale Navier-Stokes equations used in modelling fluid flow, an accurate representation of the error propagation resulting from the approximation is required. An illustrative example of quantifying this numerical error in fluid dynamics is provided by Oliver et al. (2014) and a preliminary attempt at a Bayesian formalization of the uncertainty induced is described by Oliver and Moser (2011).

The central contribution in this paper is a formalism for viewing the forward problem in the context of a Bayesian updating procedure, with updates conditional on model interrogations, and embedding the resulting uncertainty into the Bayesian hierarchy within the calibration problem. Within the forward problem, a provably consistent, first order convergent probabilistic solver for differential equations is defined. The properties of this approach are investigated in a wide variety of settings, and implications are discussed for developing a new field of *probabilistic numerics*¹ within the framework of Bayesian inference.

In particular, uncertainty is modelled about an implicitly specified differential equation solution by defining a probability model on a space of trajectories conditional on model parameters, θ , hyperparameters, Ψ_N , and interrogations, $\mathbf{f} \in \mathbb{R}^N$, of the differential equation over a discretization grid of size N . Dynamics-dependent solution uncertainty is described by the probability measure, marginalized over the sequence of auxiliary model evaluations, \mathbf{f} ,

$$[u(x, t, \theta) \mid \theta, \Psi_N] = \int [u(x, t, \theta), \mathbf{f} \mid \theta, \Psi_N] d\mathbf{f}. \quad (1)$$

The structured uncertainty quantified by (1) is illustrated in Section 4.3 in the context of a three state chaotic system whose trajectory is restricted around a region of the phase space. Figures 6a and 6b show pointwise draws from (1) for all three uncertain states and for the first state respectively, which are shown to also be confined within this region. Additionally, the probability model (1) provides a formal trade-off between solution uncertainty and computational cost, as determined by the size of the discretization grid. Figure 1 compares the exact, but a priori unknown solution with sample trajectories from the proposed probability model (1) obtained over progressively finer discretization grids. This is contrasted with a comparable traditional first order explicit numerical method using the same number of function evaluations. The proposed

¹<http://probabilistic-numerics.org>

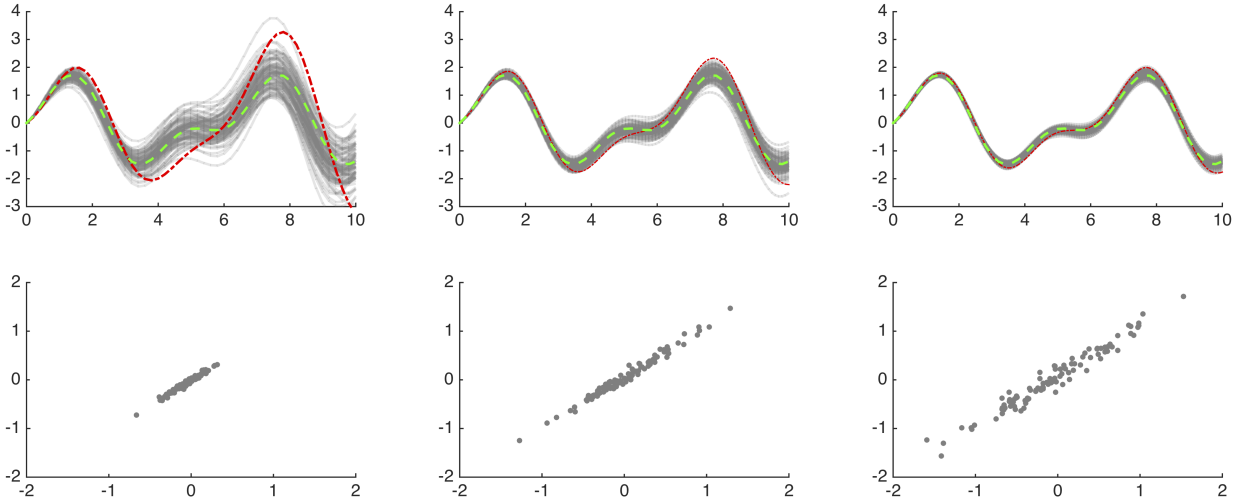


Figure 1: The top row compares a first order convergent probabilistic solver, illustrated via 100 draws (grey lines) from the marginal probability density $p\{u(\mathbf{t}, \theta) \mid \theta, \Psi_N\}$ on the dense grid \mathbf{t} , with the first order explicit Euler method (red line), and the exact solution (green line) for the ODE initial value problem (4) with $\theta = 2$ given three equally-spaced partitions of the domain $[0, 10]$ of sizes $N = 50, 100, 200$ (from left to right). The probabilistic solution characterizes uncertainty in the state for each grid size, and the exact solution lies within the high posterior density region. The bottom row shows samples from the joint distribution of the probabilistic solutions at two consecutive times, $t = [10, 11]$, $t = [30, 31]$ and $t = [50, 51]$ (from left to right). The probability model captures the structure of the discretization errors resulting in strong correlations.

probabilistic solver adequately characterises the discretization bias, and as more information is obtained about the model, our knowledge of the solution becomes more certain, concentrating eventually around the exact solution. The bottom row in Figure 1 illustrates the strong correlation in the error structure between the probabilistic solutions at consecutive time points.

The statistical *inverse problem* concerns the uncertainty in unknown model inputs, θ , given measurements of the model states. Much work in this area has been presented in the statistics literature (Bock, 1983; Brunel, 2008; Calderhead and Girolami, 2011; Campbell and Steele, 2011; Campbell and Chkrebtii, 2013; Dowd, 2007; Gugushvili and Klaassen, 2012; Ionides et al., 2006; Liang and Wu, 2008; Ramsay et al., 2007; Xue et al., 2010; Xun et al., 2013). However, inference for differential equation models lacking a closed form solution has mainly proceeded under the unverified assumption that numerical error is negligible over the entire parameter space being considered.

Using the framework of Kennedy and O’Hagan (2001), the discrepancy between the numerical approximation, \hat{u}^N , and the unobservable mathematical model, u^* , at the observation locations $(\mathbf{x}, \mathbf{t}) \in \mathcal{D}^T$ would be modelled by a discrepancy, $\delta(\mathbf{x}, \mathbf{t}) = u^*(\mathbf{x}, \mathbf{t}, \theta) - \hat{u}^N(\mathbf{x}, \mathbf{t}, \theta)$. Estimation of $\delta(\mathbf{x}, \mathbf{t})$ requires observations $y(\mathbf{x}, \mathbf{t})$ from $u^*(\mathbf{x}, \mathbf{t}, \theta)$. However, discretization error changes in form and magnitude with θ and $\delta(\mathbf{x}, \mathbf{t})$ and is agnostic to the specific form of the underlying mathematical model, which is treated as a “black box”. Consequently exploring the model uncertainty for a variety of θ requires observations for each setting or assumes $\delta(\mathbf{x}, \mathbf{t})$ is independent of θ . In the discussion of Kennedy and O’Hagan (2001), H. Wynn argues that the sensitivity equations and other underlying mathematical structures that govern the numerical approximation could also be included in the overall uncertainty analysis.

By modelling uncertainty in the unknown solution independently of the observed data, via (1), we define an additional layer in the Bayesian hierarchy within the inverse problem,

$$[\theta, u(x, t, \theta), \Psi_N \mid y(\mathbf{x}, \mathbf{t})] \propto \underbrace{[y(\mathbf{x}, \mathbf{t}) \mid u(x, t, \theta), \theta, \Sigma]}_{\text{Likelihood}} \underbrace{[u(x, t, \theta) \mid \theta, \Psi_N]}_{\text{Solution Uncertainty}} \underbrace{[\theta, \Psi_N, \Sigma]}_{\text{Prior}}. \quad (2)$$

Using the heat equation of Section 5.1 as an illustrative example, Figure 8 demonstrates the impact of

accounting for solution uncertainty in the inverse problem in (2) as a function of the discretization grid and highlights the potential for introducing model bias by ignoring it.

Throughout the paper we will make use of the mathematical framework for defining numerical problems on function spaces developed through the foundational work of Stuart (2010), Kaipio and Somersalo (2007), O’Hagan (1992), and Skilling (1991). Notationally, we will denote partial derivatives using subscripts to indicate the variable with respect to which a partial derivative is taken. For example $u_{xx} := \frac{\partial^2}{\partial x^2} u$ denotes the second partial derivative of u with respect to x . Superscripts in parentheses will denote elements of a vector, for example, $u^{(k)}$ denotes the k th element of the P -dimensional vector u . Superscripts without parentheses refer to Bayesian updates, for example, μ^k will denote the k th posterior update while u^k represents a sample from μ^k . Finally, for notational simplicity, we shall omit the dependence of the differential equation solution u on θ when the context makes this dependence clear.

1.1 Differential equation models under consideration

Our work addresses modelling challenges that arise for the following classes of deterministic ordinary and partial differential equation models, for which analytical solutions are generally not available.

Ordinary Differential Equation (ODE) models represent the evolution of system states $u \in \mathcal{U}$ over time $t \in [a, b]$ implicitly through the equation $u_t(t, \theta) = f\{t, u(t, \theta), \theta\}$. The standard assumptions about the known function f are that it is continuous in the first argument and Lipschitz continuous in the second argument, ensuring the existence and uniqueness of a solution corresponding to a known initial state $u^*(a)$. Inputs and boundary constraints define several model variants.

The *Initial Value Problem* (IVP) of order one models time derivatives of system states as known functions of the states constrained to satisfy initial conditions, $u^*(a)$,

$$\begin{cases} u_t(t) = f\{t, u(t), \theta\}, & t \in [a, b], \\ u(a) = u^*(a). \end{cases} \quad (3)$$

The existence of a solution is guaranteed under mild conditions (see for example, Butcher, 2008; Coddington and Levinson, 1955). Such models may be high dimensional and contain other complexities such as algebraic components, functional inputs, or higher order terms. Higher order initial value problems may be restated as a system of first order equations by defining additional states. The following simple example of a second order initial value problem will be used to illustrate our approach:

$$\begin{cases} u_{tt}(t, \theta) = \sin(\theta t) - u, & t \in [0, 10], \\ u(a) = -1, \\ u_t(0, \theta) = 0. \end{cases} \quad (4)$$

The availability of the exact solution, $u(t, \theta) = \{-\theta^2 \cos(t) + \theta \sin(t) - \sin(\theta t) + \cos(t)\} / (\theta^2 - 1)$, allows for comparison in Figures 1 and 2.

While IVP models specify a fixed initial condition on the system states, the *Mixed Boundary Value Problem* (MBVP) may constrain different states at different time points. Typically these constraints are imposed at the boundary of the time domain. For example, the two state mixed boundary value problem is,

$$\begin{cases} [u_t(t), v_t(t)] = f\{t, [u(t), v(t)], \theta\}, & t \in [a, b], \\ \phi\{v(a), u(b)\} = 0, \end{cases} \quad (5)$$

and can be straightforwardly generalized to higher dimensions and extrapolated beyond the final time point b . Whereas a unique IVP solution exists under relatively mild conditions, imposing mixed boundary constraints can result in multiple solutions (e.g. Keller, 1968) introducing possible problems for parameter estimation.

The *Delay Initial Function Problem* (DIFP) generalizes the initial constraint of IVPs to an initial function, $\phi(t)$, thereby relating the derivative of a process to both present and past states at lags $\tau_j \in [0, \infty)$,

$$\begin{cases} u_t(t) = f\{t, u(t - \tau_1), \dots, u(t - \tau_d), \theta\}, & t \in [a, b], \\ u(t) = \phi(t), & t \in [a - \max_j(\tau_j), a]. \end{cases} \quad (6)$$

DIFPs are well suited to describing biological and physical dynamics that take time to propagate through systems. However, they pose challenges to numerical techniques due to potentially large and structured truncation error (Bellen and Zennaro, 2003).

Partial Differential Equation (PDE) models represent the derivative of states with respect to multiple arguments, for example time and spatial variables. PDE models are ubiquitous in the applied sciences, where they are used to study a variety of phenomena, from animal movement, to the propagation pattern of a pollutant in the atmosphere. The main classes of PDE models are based on elliptic, parabolic and hyperbolic equations. Further adding to their complexity, functional boundary constraints and initial conditions make PDE models more challenging, while their underlying theory is less developed compared to ODE models (Polyanin and Zaitsev, 2004).

1.2 Contributions and Outline of the Paper

A new approach is developed to characterize uncertainty in the solution of differential equation models with unknown closed form solutions. Instead of considering numerical error bounds around a deterministic approximation, we build a probability model describing knowledge about the exact but a priori unknown solution, u^* , and update our beliefs by conditioning on model interrogations obtained over a discrete partition of the domain, \mathcal{D} . Our contribution formalizes and substantially expands the ideas first presented by Skilling (1991), yielding a general class of probability models for solution uncertainty. Furthermore, by marginalization over model interrogations, our approach quantifies the model dependent structure of discretization uncertainty. Beginning with a Gaussian Process prior model for the differential equation solution and its derivative in Section 2, the probabilistic solver we present is defined in terms of a sequential Bayesian updating procedure in Section 3. Proof of consistency and first order convergence to the exact solution are given in Section 3.3. We then show how our approach can be set up to achieve computational complexity of the same order as comparably sampled explicit numerical solvers (Section 3.2). The proposed approach is then used to model solution uncertainty for a wide class of ODE and PDE problems, including mixed boundary value problems exhibiting multiplicity of solutions, delay initial function problems with partially observed initial functions, and stiff, chaotic PDEs in Section 4. This section also illustrates the scalability of the probabilistic solver by building a model of discretization uncertainty for the Navier-Stokes system via pseudo spectral projection, involving the solution of over 16,000 coupled stiff ordinary differential equations. Section 5 adopts a forward-simulation sampling approach that allows propagation of discretization uncertainty within the inferential procedure for inverse problems. Discussion of various extensions and relationships to probabilistic numerics is given in Section 6. MATLAB implementations of all examples are available for download at <http://web.warwick.ac.uk/PODES>.

2 Prior Model for a Fixed but Unknown Solution

This section begins by setting out constraints and initial beliefs regarding the unknown function, $u^* \in \mathcal{U}$, satisfying an ODE initial value problem on the domain $\mathcal{D} = [a, b] \subset \mathbb{R}$, and a PDE boundary value problem on a more general domain $\mathcal{D} \subset \mathbb{R}^d$. A convenient way of making prior probability statements on such infinite dimensional objects is through a Gaussian process (GP) model on a space of trajectories (Rasmussen and Williams, 2006; Stuart, 2010). This section describes how to incorporate reasonable boundary and regularity assumptions into a GP prior model for the unknown solution, u^* . These prior beliefs are updated in Section 3 by conditioning on a sample of auxiliary information obtained by interrogating the differential equation model over a size N partition of the domain \mathcal{D} according to a chosen sampling scheme.

2.1 GP prior on the solution of an ODE initial value problem

The flexibility of Gaussian process (GP) priors is exploited to describe prior uncertainty jointly for the solution and its time derivative, $[u_t, u]$ as defined uniquely by covariance function, $[C_t^0, C^0]$, and initial mean function, $[m_t^0, m^0]$.

The prior mean function is chosen to satisfy the constraint $\int_a^t m_t^0(z) dz = m^0(t)$. A convolution of kernels provides a flexible approach for defining the covariance structure between evaluation time points t_j and t_k

(see, for example, Higdon, 1998, 2002). Convolution of a square integrable kernel $R_\lambda : \mathbb{R} \times \mathbb{R} \rightarrow \mathbb{R}$ with itself establishes a positive-definite covariance operator for u_t ,

$$C_t^0(t_j, t_k) = \alpha^{-1} \int_{\mathbb{R}} R_\lambda(t_j, z) R_\lambda(t_k, z) dz,$$

with length-scale $\lambda > 0$ and prior precision $\alpha > 0$. From this, a marginal covariance operator on the state, C^0 , is obtained by integrating C_t^0 with respect to evaluation points t_j and t_k or, equivalently, by convolving the integrated kernel $Q_\lambda(t_j, t_k) = \int_a^{t_j} R_\lambda(z, t_k) dz$ with itself:

$$C^0(t_j, t_k) = \alpha^{-1} \int_{\mathbb{R}} Q_\lambda(t_j, z) Q_\lambda(t_k, z) dz.$$

The cross-covariance terms are defined analogously as $\int_a^{t_j} C_t^0(z, t_k) dz := \alpha^{-1} \int_{\mathbb{R}} Q_\lambda(t_j, z) R_\lambda(t_k, z) dz$ and $\int_a^{t_k} C_t^0(t_j, z) dz = \alpha^{-1} \int_{\mathbb{R}} R_\lambda(t_j, z) Q_\lambda(t_k, z) dz$, noting that each is the adjoint of the other. Several choices of R_λ and the required integrals and convolutions for defining covariances in this way are provided in the Appendix (Section 7.5). The initial joint GP prior probability measure, μ^0 , on the solution at a vector of evaluation times \mathbf{t}_k and its time derivative at a possibly different vector of evaluation times \mathbf{t}_j , conditional on hyperparameters $\Psi_N = [m_t^0, m^0, \alpha, \lambda]$ is given by,

$$\begin{bmatrix} u_t(\mathbf{t}_j) \\ u(\mathbf{t}_k) \end{bmatrix} \Big| \Psi_N \sim \mu^0 = \mathcal{GP} \left(\begin{bmatrix} m_t^0(\mathbf{t}_j) \\ m^0(\mathbf{t}_k) \end{bmatrix}, \begin{bmatrix} C_t^0(\mathbf{t}_j, \mathbf{t}_j) & \int_a^{\mathbf{t}_k} C_t^0(\mathbf{t}_j, \mathbf{z}) d\mathbf{z} \\ \int_a^{\mathbf{t}_k} C_t^0(\mathbf{z}, \mathbf{t}_j) d\mathbf{z} & C^0(\mathbf{t}_k, \mathbf{t}_k) \end{bmatrix} \right). \quad (7)$$

The choice of hyperparameters α and λ will be discussed in Section 3.4. The kernel R_λ reflects any prior assumptions regarding the smoothness of the unknown solution's time derivative, u_t^* . The usual recommendation from the function estimation literature is adopted (see, for example, Rasmussen and Williams, 2006) to choose a kernel whose smoothness is as close as possible to the hypothesized regularity of the unknown function, in this case u_t^* .

An additional requirement for the ODE initial value problem is that the boundary value conditions are satisfied. There are at least two ways to ensure that the initial state $u^*(a)$ is enforced a priori. One option is to begin with an arbitrary GP model for the state and condition on the exact initial state, $u^*(a)$. This approach has the flexibility of easily enforcing complex boundary conditions. Alternatively, one may constrain the prior (7) by construction, modelling the state as an integrated derivative process. In this case, the constant of integration will satisfy the boundary condition if the prior mean satisfies the constraint $m^0(a) = u^*(a)$. In this paper we choose to employ the latter prior model, since its construction directly mirrors the structure of the ODE initial value problem. For more advanced applications such as PDE problems in which more complex boundary conditions are enforced, one can also employ a combination of these two approaches to prior specification. The above prior modelling strategies may also be generalized to initial value problems of order greater than one by defining the prior jointly on the state and the required higher order derivatives. A more convenient approach however is to convert the higher order ODE initial value problem into an equivalent first order system by defining additional states. Priors on these states may then either be modelled independently of one another, or with a prior cross-covariance structure between states if such information is available.

2.2 GP prior on the solution of a PDE boundary value problem

Similarly, the prior belief is modelled about the fixed but unknown solution and partial derivatives of a PDE boundary value problem by defining a probability measure over multivariate trajectories, as well as first or higher order derivatives with respect to spatial inputs. The prior structure will depend on the form of the PDE model under consideration. As an illustration, consider the parabolic heat equation on the spatio-temporal domain $\mathcal{D} = [a^x, b^x] \times [a^t, b^t]$, describing the heat diffusion over time along a single spatial dimension implicitly via,

$$\begin{cases} u_t(x, t) &= \kappa u_{xx}(x, t), & t \in [a^t, b^t], & x \in [a^x, b^x], \\ u(x, t) &= \sin(x\pi), & t = a^t, & x \in [a^x, b^x], \\ u(x, t) &= 0, & t \in [a^t, b^t], & x \in \{a^x, b^x\}, \end{cases} \quad (8)$$

where the boundaries of the domain in each spatio-temporal dimension may be parametrized with respect to the remaining dimension coordinates. One modelling choice for extending the prior covariance to a spatio-temporal domain is to assume separability by defining covariances over time and space independently. Accordingly we choose temporal kernel R_λ as in Section 2.1 and let $R_\nu : \mathbb{R} \times \mathbb{R} \rightarrow \mathbb{R}$ be a possibly different spatial kernel function with length-scale ν . We integrate the spatial kernel once to obtain $Q_\nu(x_g, x_\ell) = \int_{a^x}^{x_g} R_\nu(z, x_\ell) dz$ and twice to obtain $S_\nu(x_g, x_\ell) = \int_{a^x}^{x_\ell} Q_\nu(z, x_\ell) dz$. The covariance structures between temporal and spatial evaluation points x_1, x_2, t_1 , and t_2 are obtained from the process convolution formulation with temporal and spatial prior precision parameters α and β respectively, as follows,

$$\begin{aligned} C_{xx}^0([x_1, t_1], [x_2, t_2]) &= \alpha^{-1} \beta^{-1} \int_{\mathbb{R}} R_\nu(x_1, z) R_\nu(x_2, z) dz \int_{\mathbb{R}} Q_\lambda(t_1, w) Q_\lambda(t_2, w) dw, \\ C_t^0([x_1, t_1], [x_2, t_2]) &= \alpha^{-1} \beta^{-1} \int_{\mathbb{R}} S_\nu(x_1, z) S_\nu(x_2, z) dz \int_{\mathbb{R}} R_\lambda(t_1, w) R_\lambda(t_2, w) dw, \\ C^0([x_1, t_1], [x_2, t_2]) &= \alpha^{-1} \beta^{-1} \int_{\mathbb{R}} S_\nu(x_1, z) S_\nu(x_2, z) dz \int_{\mathbb{R}} Q_\lambda(t_1, w) Q_\lambda(t_2, w) dw, \end{aligned}$$

with cross-covariances defined analogously.

The mean function and above covariance specification uniquely determine the joint GP prior, μ^0 , on the state and its partial derivatives given hyperparameters Ψ_N , which include $\alpha, \beta, \lambda, m_{xx}^0, m_t^0, m^0$, at vectors of temporal and spatial evaluation points $\mathbf{x}_1, \mathbf{x}_2, \mathbf{x}_3, \mathbf{t}_1, \mathbf{t}_2$, and \mathbf{t}_3 as:

$$\begin{bmatrix} u_{xx}(\mathbf{x}_1, \mathbf{t}_1) \\ u_t(\mathbf{x}_2, \mathbf{t}_2) \\ u(\mathbf{x}_3, \mathbf{t}_3) \end{bmatrix} \Big| \Psi_N \sim \mu^0 = \mathcal{GP} \left(\begin{bmatrix} m_{xx}^0(\mathbf{x}_1, \mathbf{t}_1) \\ m_t^0(\mathbf{x}_2, \mathbf{t}_2) \\ m^0(\mathbf{x}_3, \mathbf{t}_3) \end{bmatrix}, C \right), \quad (9)$$

with covariance defined by,

$$C = \begin{bmatrix} C_{xx}^0([\mathbf{x}_1, \mathbf{t}_1], [\mathbf{x}_1, \mathbf{t}_1]) & \int_{a^t}^{\mathbf{x}_1} \int_{a^z}^z \frac{\partial}{\partial \mathbf{t}_2} C_{xx}^0([w, \mathbf{t}_1], [\mathbf{x}_2, \mathbf{t}_2]) dw dz & \int_{a^{\mathbf{x}_3}}^{\mathbf{x}_3} \int_{a^x}^z C_{xx}^0([\mathbf{x}_1, \mathbf{t}_1], [w, \mathbf{t}_3]) dw dz \\ \int_{a^t}^{\mathbf{x}_1} \int_{a^z}^z \frac{\partial}{\partial \mathbf{t}_2} C_{xx}^0([\mathbf{x}_2, \mathbf{t}_2], [w, \mathbf{t}_1]) dw dz & C_t^0([\mathbf{x}_2, \mathbf{t}_2], [\mathbf{x}_2, \mathbf{t}_2]) & \int_{a^{\mathbf{x}_3}}^{\mathbf{x}_3} \int_{a^x}^z C_t^0([\mathbf{x}_2, \mathbf{t}_2], [\mathbf{x}_3, w]) dw \\ \int_{a^{\mathbf{x}_3}}^{\mathbf{x}_3} \int_{a^x}^z C_{xx}^0([w, \mathbf{t}_3], [\mathbf{x}_1, \mathbf{t}_1]) dw dz & \int_{a^t}^{\mathbf{t}_3} C_t^0([\mathbf{x}_3, w], [\mathbf{x}_2, \mathbf{t}_2]) dw & C^0([\mathbf{x}_3, \mathbf{t}_3], [\mathbf{x}_3, \mathbf{t}_3]) \end{bmatrix}.$$

When integrated covariances are available in closed form (Appendix, Section 7.5), any required covariance matrices can be computed directly.

3 Updating Prior Beliefs for Fixed but Unknown ODE Solution

We now return to our goal of exploring the forward model for u^* . Rather than considering a traditional numerical approximation u^N , we shall examine the probability model defined in equation (1), which describes our degree of belief about the function u^* as we produce and assimilate model evaluations at subsequent time steps. That is, recovering the model explicitly is viewed as a function estimation problem, algorithmically defined via a Bayesian updating procedure. Functionals of the marginal probability distribution (1) may then be studied empirically based on samples of realized individual trajectories.

Model interrogations are generated sequentially based on state samples drawn from progressively refined prior models, in order to accommodate fast changing dynamics. This section begins by expanding on these function estimation steps with full details of the Bayesian updating algorithm. Section 3.2 examines modelling choices for which this procedure can attain computational complexity of $O(N)$, while Section 3.3 proves the consistency and first order convergence properties of this approach. Choice of hyperparameters is addressed in Section 3.4.

3.1 Model Updating Based on Interrogations from Sampled Auxiliary Variables

This section describes a sequential auxiliary variable sampling scheme used to interrogate the model after each update. Model interrogations occur at times $a = s_1 < s_2 < \dots < s_N = b$ and model evaluations occur at a possibly different vector of times of interest, \mathbf{t} . There are many ways to generalize the basic one-step-ahead sampling scheme, some of which are discussed in Section 6.

3.1.1 First update

The derivative of the exact solution on the boundary, $s_1 = a$, can be obtained exactly by evaluating the ODE model (3) at the known initial condition $u^*(s_1)$ as,

$$f_1 = f \{s_1, u^*(s_1), \theta\} = u_t^*(s_1).$$

Thus the first update of the prior probability measure μ^0 in (7) is performed by conditioning on the exact derivative f_1 . This yields the joint conditional predictive probability measure at the vectors of evaluation times \mathbf{t}_j and \mathbf{t}_k

$$\begin{bmatrix} u_t(\mathbf{t}_j) \\ u(\mathbf{t}_k) \end{bmatrix} \Big| f_1, \Psi_N \sim \mu^1 = \mathcal{GP} \left(\begin{bmatrix} m_t^1(\mathbf{t}_j) \\ m^1(\mathbf{t}_k) \end{bmatrix}, \begin{bmatrix} C_t^1(\mathbf{t}_j, \mathbf{t}_j) & \int_a^{\mathbf{t}_k} C_t^1(\mathbf{t}_j, \mathbf{z}) d\mathbf{z} \\ \int_a^{\mathbf{t}_j} C_t^1(z, \mathbf{t}_k) dz & C^1(\mathbf{t}_k, \mathbf{t}_k) \end{bmatrix} \right), \quad (10)$$

with marginal derivative mean and covariance,

$$\begin{aligned} m_t^1(\mathbf{t}_k) &= m_t^0(\mathbf{t}_k) + C_t^0(\mathbf{t}_k, s_1) C_t^0(s_1, s_1)^{-1} \{f_1 - m_t^0(s_1)\}, \\ C_t^1(\mathbf{t}_k, \mathbf{t}_k) &= C_t^0(\mathbf{t}_k, \mathbf{t}_k) - C_t^0(\mathbf{t}_k, s_1) C_t^0(s_1, s_1)^{-1} C_t^0(s_1, \mathbf{t}_k), \end{aligned}$$

and with marginal state mean, covariance, and derivative cross-covariances obtained by integration (see Appendix, Section 7.2). We refer to this predictive probability measure as μ^1 , or the *first update* of the algorithm. We will take μ^1 to be the prior for the next update of the algorithm.

3.1.2 Second update

The derivative of the exact solution is unknown beyond the boundary. We therefore introduce the random variable f_2 , representing a model interrogation at the subsequent time step $s_2 > s_1$. Its realization is obtained by firstly drawing a realization from the marginal predictive distribution over the state in μ^1 at time s_2 ,

$$u^1(s_2) \mid f_1, \Psi_N \sim N(m^1(s_2), C^1(s_2, s_2)).$$

and secondly transforming the sampled state $u^1(s_2)$ into the derivative space by evaluating the ODE model (3), as,

$$f_2 = f \{s_2, u^1(s_2), \theta\}.$$

In order to update μ^1 given f_2 , we require a likelihood model for the discrepancy between f_2 and the time derivative of the exact but unknown solution, $u_t^*(s_2)$ at time s_2 . Without prior knowledge of the differential equation solution, we are uncertain about the distribution of this transformed random variable and must define an appropriate alternative likelihood, for which we may consider the following facts:

1. The equality $u_t^1(s_2) = f \{s_2, u^1(s_2), \theta\}$ is satisfied only when the sampled $u^1(s_2)$ coincides with the exact solution $u^*(s_2)$. This corresponds to a discrepancy of zero;
2. The function f is smooth (Lipschitz continuous) in the second argument, therefore discrepancy decreases smoothly with decreasing uncertainty in the derivative of the sampled state realization $u^1(s_2)$;

These facts suggest a likelihood model for f_2 with a single mode at $f_2 = u_t(s_2)$. Unless there is additional information about the specific model of interest, it is reasonable to assume the error in f_2 to be spherically symmetric about $u_t(s_2)$. Therefore, a Gaussian likelihood is chosen with mean $u_t(s_2)$ and variance equal to the predictive variance of the derivative, $u_t(s_2)$, (Skilling, 1991) such that,

$$f_2 \mid u_t \sim N \{u_t(s_2), C_t^1(s_2, s_2)\}. \quad (11)$$

We may now update μ^1 by conditioning on the interrogation f_2 under the error model (11) to obtain the predictive probability measure at the vectors of evaluation times \mathbf{t}_j and \mathbf{t}_k

$$\begin{bmatrix} u_t(\mathbf{t}_j) \\ u(\mathbf{t}_k) \end{bmatrix} \Big| f_2, \Psi_N \sim \mu^2 = \mathcal{GP} \left(\begin{bmatrix} m_t^2(\mathbf{t}_j) \\ m^2(\mathbf{t}_k) \end{bmatrix}, \begin{bmatrix} C_t^2(\mathbf{t}_j, \mathbf{t}_k) & \int_a^{\mathbf{t}_k} C_t^2(\mathbf{t}_j, z) dz \\ \int_a^{\mathbf{t}_j} C_t^2(z, \mathbf{t}_k) dz & C^2(\mathbf{t}_k, \mathbf{t}_k) \end{bmatrix} \right). \quad (12)$$

Setting $g_2 = 2C_t^1(s_2, s_2)$, the marginal derivative mean and covariance at the vector of evaluation times \mathbf{t}_j are given by,

$$\begin{aligned} m_t^2(\mathbf{t}_j) &= m_t^1(\mathbf{t}_j) + C_t^1(\mathbf{t}_j, s_2) g_2^{-1} \{f_2 - m_t^1(s_2)\}, \\ C_t^2(\mathbf{t}_j, \mathbf{t}_j) &= C_t^1(\mathbf{t}_j, \mathbf{t}_j) - C_t^1(\mathbf{t}_j, s_2) g_2^{-1} C_t^1(s_2, \mathbf{t}_j), \end{aligned}$$

with state mean, covariance, and derivative cross-covariances obtained analytically via integration of the kernel functions defining our Gaussian process.

3.1.3 Subsequent updates

Subsequent updates, $2 < n \leq N$, begin by drawing a sample $u^{n-1}(s_n)$ at time s_n from the marginal predictive posterior μ^{n-1} over the state (these auxiliary samples are illustrated by circles in Figure 2). A realization of the interrogation f_n is then constructed by transforming the sampled state via the differential equation model. The update is then performed relative to the prior μ^{n-1} , by assimilating f_n under the Gaussian error model,

$$f_n | u_t(s_n) \sim N \{u_t(s_n), C^{n-1}(s_n, s_n)\}, \quad 1 \leq n \leq N. \quad (13)$$

Defining $g_n = 2C_t^{n-1}(s_n, s_n)$, the resulting joint predictive probability measure is Gaussian with derivative mean and covariance:

$$\begin{aligned} m_t^n(\mathbf{t}_j) &= m_t^{n-1}(\mathbf{t}_j) + C_t^{n-1}(\mathbf{t}_j, s_n) g_n^{-1} \{f_n - m_t^{n-1}(s_n)\}, \\ C_t^n(\mathbf{t}_j, \mathbf{t}_k) &= C_t^{n-1}(\mathbf{t}_j, \mathbf{t}_k) - C_t^{n-1}(\mathbf{t}_j, s_n) g_n^{-1} C_t^{n-1}(s_n, \mathbf{t}_k), \end{aligned} \quad (14)$$

and with state mean and covariances, as well as derivative cross-covariances again obtained analytically. Here the state and derivative, u_t and u respectively, may be of arbitrary dimension. We also note that equation (15) results in a sparse, band diagonal matrix when a covariance structure is chosen with bounded support.

After all N updates have been performed, we obtain a joint posterior probability distribution μ^N for the unknown solution and its derivative, conditional on realizations of one trajectory of the auxiliary random variable $\mathbf{f} \in \mathbb{R}^N$. Sampling interrogation trajectories $\mathbf{f} \in \mathbb{R}^N$ with their corresponding states yields a realization from the probability model (1). It is here that nonlinear system dynamics result in a strongly non-Gaussian error structure, as illustrated in section 4.3. This sampling strategy is described in Algorithm 1, yielding realized trajectories from the forward model (1) over a desired grid $\mathbf{t} = [t_j, \dots, t_T]$. Five draws from the joint distribution of μ^n and the auxiliary variable f_n at iterations $n = 12, 24, 36, 48$ are illustrated in the second through fifth rows of Figure 2 for the second-order ODE initial value problem (4). For notational simplicity, we will hereafter assume that the temporal locations of interest, \mathbf{t} , form a subset of the discretization grid locations, \mathbf{s} . A general version of this algorithm, sampling the state at arbitrary locations, \mathbf{t} , is provided in the on-line supplement available at <http://web.warwick.ac.uk/PODES>.

3.2 Computational complexity

When solving differential equations, knowledge about the solution can be modelled by a process with compactly-supported covariance structure; indeed, most deterministic numerical methods make the analogous assumption that the approximation at each time step depends on derivative evaluations of the system only at the previous $M \geq 1$ time steps. This assumption both adds flexibility for modelling very fast-changing dynamics and drastically reduces computational expenditure in the proposed probabilistic solver.

Under a compactly supported covariance structure, Algorithm 1 involves only $O(N)$ operations by allowing truncation of the weight matrices employed in the mean and variance updates. More precisely, if the covariance has support of length 2ℓ and the step number, $M = \lfloor \frac{\ell}{h} \rfloor$ is set as a function of the maximum step size h , then the number of operations required for one evaluation of Algorithm 1 is proportional to the number of time steps N times the constant M . For example, the application in Section 4.4 to probabilistically modelling solution uncertainty for the Navier-Stokes equations of fluid dynamics, which comprise over 16,000 coupled ODEs, is made computationally feasible by assuming bounded support covariance structure; indeed, even simply storing matrices of model evaluations would quickly exceed computer memory limits.

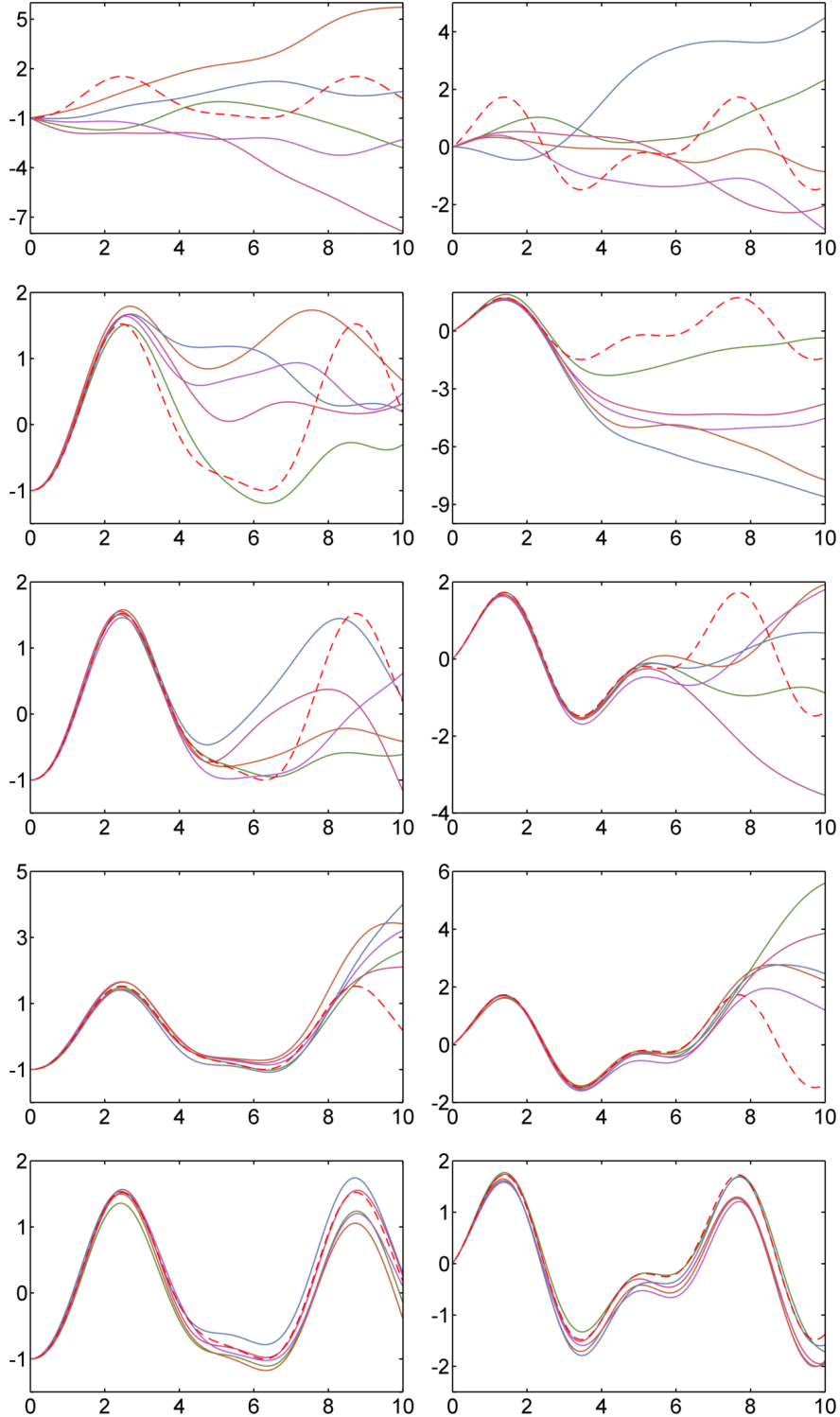


Figure 2: Each figure shows five draws (solid lines) from the marginal predictive probability measure μ^n on the state (right) and its derivative (left) for the second-order ODE initial value problem (4) after $n = 0, 12, 24, 36, 48$ iterations of Algorithm 1. Samples from the predictive distribution over the state at the next time step are represented by circles in each plot. The discretization grid is an equally spaced domain partition of size $N = 50$. The exact solution is shown as a dotted line for comparison.

Algorithm 1 Draw one sample from the forward model (1) using a probabilistic solver evaluated over the grid $\mathbf{t} = [t_j, \dots, t_T]$ for the solution of an ODE initial value problem with initial state $u^*(a)$ given θ, Ψ_N , and discretization grid $\mathbf{s} = [s_1, \dots, s_N]$.

At time $s_1 = a$, Initialize the derivative $\mathbf{f}_1 = f\{s_1, u^*(a), \theta\}$, and define m^0, m_t^0, C^0, C_t^0 as above;

for $n = 1 : N$ **do**

If $n = 1$, set $g_1 = C_t^0(s_1, s_1)$, otherwise set $g_n = 2C_t^{n-1}(s_n, s_n)$; Compute for each modelled system component,

$$\begin{aligned} m^n(\mathbf{s}) &= m^{n-1}(\mathbf{s}) + g_n^{-1} \int_a^{\mathbf{s}} C_t^{n-1}(z, s_n) dz \{ \mathbf{f}_n - m_t^{n-1}(s_n) \}, \\ m_t^n(\mathbf{s}) &= m_t^{n-1}(\mathbf{s}) + g_n^{-1} C_t^{n-1}(\mathbf{s}, s_n) \{ \mathbf{f}_n - m_t^{n-1}(s_n) \}, \\ C^n(\mathbf{s}, \mathbf{s}) &= C^{n-1}(\mathbf{s}, \mathbf{s}) - g_n^{-1} \int_a^{\mathbf{s}} C_t^{n-1}(z, s_n) dz \left\{ \int_a^{\mathbf{s}} C_t^{n-1}(z, s_n) dz \right\}^\top, \\ C_t^n(\mathbf{s}, \mathbf{s}) &= C_t^{n-1}(\mathbf{s}, \mathbf{s}) - g_n^{-1} C_t^{n-1}(\mathbf{s}, s_n) C_t^{n-1}(s_n, \mathbf{s}), \\ \int_a^{\mathbf{s}} C_t^n(z, \mathbf{s}) dz &= \int_a^{\mathbf{s}} C_t^{n-1}(z, \mathbf{s}) dz - g_n^{-1} \int_a^{\mathbf{s}} C_t^{n-1}(z, s_n) dz C_t^{n-1}(s_n, \mathbf{s}); \end{aligned}$$

if $n < N$ **then**

sample step ahead realization $u^n(s_{n+1})$ from the predictive distribution on the state for each modelled system component,

$$u^n(s_{n+1}) \sim p\{u(s_{n+1}) \mid \mathbf{f}_n, \Psi_N\} = \mathcal{N}\{u(s_{n+1}) \mid m^n(s_{n+1}), C^n(s_{n+1}, s_{n+1})\},$$

and obtain realizations of the auxiliary variable by evaluating the ODE model at the sampled point,

$$\mathbf{f}_{n+1} = f\{s_{n+1}, u^n(s_{n+1}), \theta\};$$

end if

end for

Return $[u(t_j), \dots, u(t_T)] \sim \mathcal{GP}\{m^N(\mathbf{t}), C^N(\mathbf{t}, \mathbf{t})\}$, where $\mathbf{t} \subset \mathbf{s}$.

In contrast, when employing a covariance structure with unbounded support, Algorithm 1 attains computational complexity proportional to the cube of the number of time steps, i.e. $O(N^3)$ operations, since the number of operations can be written as a finite sum over $1 \leq n \leq N$ with each n th iteration containing an order $O(n^2)$ matrix multiplication.

The proposed approach formally allows the user to make a trade-off between a probabilistic representation of uncertainty in the solution trajectory and the computational expenditure associated with selecting the size of the discretization grid. Within the forward problem, the ability to quantify discretization uncertainty in a probabilistic manner allows the possibility of using coarser grids than might otherwise be required by deterministic numerical techniques, while still appropriately accounting for discretization related bias. Such discretization uncertainty may then be propagated through the rest of the inference procedure, in particular in inverse problems, where the distribution of interest is the posterior over some model parameters, θ . Additionally, information from the data and the model can be used to infer appropriate values for the hyperparameters, Ψ_N . The dependent relationship between Ψ_N and θ is highlighted in the inference example in Section 5.2.

3.3 Convergence

We now consider the rate at which the stochastic process with probability distribution (1) generated via Algorithm 1 concentrates around the true solution.

Theorem 3.1. *Consider a derivative function $f(\cdot, \cdot, \theta) : [a, b] \times \mathbb{R} \rightarrow \mathbb{R}$ that is continuous in the first argument and Lipschitz continuous in the second argument. The stochastic process with probability distribution (1) obtained using Algorithm 1 under a covariance kernel satisfying conditions (28) and (29) in Appendix 7.4, converges in L^1 to the unique solution satisfying (3) at a rate proportional to the decrease in the maximum step size.*

The order of convergence is as fast as the reduction of truncation error for the analogously sampled one-step explicit Euler method. A proof of the above theorem is provided in the Appendix (Section 7.3).

3.4 The choice of hyperparameters

Having demonstrated solution uncertainty quantification for differential equations in terms of Bayesian function estimation, we next turn our attention to the choice of covariance hyperparameters. This important consideration must be based on prior knowledge of the uncertainty in the solution as well as the number and location of the model evaluations used to update our degree of belief about u^* . Moreover, as with many nonparametric function estimation problems, asymptotic results on convergence may be used to guide our choice of covariance hyperparameters within the forward problem. For example, for the explicit first-order sampling scheme, the result of Theorem 3.1 suggests setting the prior variance, $1/\alpha$, and the length-scale, λ , proportionally to the maximum distance, h , between subsequent discretization grid locations. The constant of proportionality may be chosen based on the shape of the covariance kernel selected (see, for example, Appendix, Section 7.5).

Importantly, the choice of hyperparameters within the forward problem allows incorporation of prior knowledge into our probability model for the unknown solution, and allows us to infer posterior densities over hyperparameters within the setting of an inverse problem. In contrast, deterministic numerical differential equation solvers effectively fix the analogues of these hyperparameters by choice of the numerical method used, such as the quadrature rule or the step number, both within the forward and inverse problems. In section 5 a Markov chain Monte Carlo sampler is used to obtain posterior draws over hyperparameters within the inverse problem given transformed observations of the states contaminated with error. We illustrate how this approach allows for data driven adaptation of hyperparameter settings over the space, Θ , of model parameters.

4 Modeling the Solution of Other Forward Problems

This section extends probabilistic updating of solution uncertainty to a variety of forward models. In particular, we examine a PDE, an ill-conditioned mixed boundary value problem, a stiff, high-dimensional ODE initial value problem, and systems exhibiting chaotic dynamics.

4.1 Updating Prior Beliefs for Fixed but Unknown PDE Solution

PDE models are ubiquitous in the applied sciences, where they are used to study a variety of phenomena, from animal movement, to the propagation pattern of a pollutant in the atmosphere. The goal is to first model uncertainty about the solution through the prior (9) defined over time and space using a product covariance structure as described in Section 2. The prior may then be updated by conditioning on PDE model interrogations corresponding to approximate time derivatives at each discretization grid location, dependent on sequentially sampled realizations from the predictive posterior distribution over the second order spatial derivatives. The sequential updating scheme presented in Algorithm 1 may be generalized to characterize the discretization uncertainty in both the temporal and spatial domains for PDE boundary value problems.

Due to the variety of PDE boundary value problem types, we illustrate the extension to PDEs and the feasibility of modelling discretization uncertainty in both the spatial and temporal domains by applying our model to the parabolic Heat Equation PDE boundary value problem (8) via Algorithm 2. We consider the heat equation on the spatio-temporal domain $\mathcal{D} = [0, 1] \times [0, 0.25]$, describing heat diffusion over time along a single spatial dimension implicitly via (8).

Consider the forward problem of solving this system given a conductivity parameter of $\kappa = 1$ and an initial function $u^*(x, 0) = \sin(x\pi)$, $x \in [0, 1]$. In Figure 3 the exact solution is compared with the probability model of its knowledge given two different grids: a coarse discretization of 15 points in the spatial domain and 50 points in the temporal domain, and a finer discretization of 29 points in the spatial domain and 100 points in the temporal domain. The simulations illustrate that as the mesh size becomes finer, the uncertainty in the solution decreases, in agreement with the consistency result presented in Section 3.3 for ODE initial value problems.

Algorithm 2 Sampling u from the probabilistic solver evaluated over the grid $\mathbf{X} \otimes \mathbf{T}$ for the heat equation, defined in equation (8), given κ, Ψ_N, N, M .

Define temporal discretization grid, $\mathbf{s} = [s_1, \dots, s_N]$, and for each s_n define spatial discretization grid $\mathbf{z}_n = [z_{1,n}, \dots, z_{M,n}]$, $1 \leq n \leq N$, and construct the $N \times M$ design matrix $\mathbf{Z} = [\mathbf{z}_1; \dots; \mathbf{z}_N]$;

At time $s_1 = 0$ initialize the second spatial derivative using the given boundary function and compute the temporal derivative $\mathbf{f}_1 = \kappa [u_{xx}(z_{1,1}, s_1), \dots, u_{xx}(z_{M,1}, s_1)]$;

Define the prior covariance as in (9);

for $n = 1 : N$ **do**

If $n = 1$, set $G_1 = C_t^0([\mathbf{z}_1, s_1], [\mathbf{z}_1, s_1])$, otherwise set $G_n = 2C_t^{n-1}([\mathbf{z}_n, s_n], [\mathbf{z}_n, s_n])$; Compute,

$$\begin{aligned} m_{xx}^n(\mathbf{Z}, \mathbf{s}) &= m_{xx}^{n-1}(\mathbf{Z}, \mathbf{s}) + \frac{\partial^2}{\partial \mathbf{Z}^2} \int_{a^t}^{\mathbf{s}} C_t^{n-1}([\mathbf{Z}, t], [\mathbf{z}_n, s_n]) dt G_n^{-1} \{ \mathbf{f}_n - m_t^{n-1}(\mathbf{z}_n, s_n) \}, \\ m_t^n(\mathbf{Z}, \mathbf{s}) &= m_t^{n-1}(\mathbf{Z}, \mathbf{s}) + C_t^{n-1}([\mathbf{Z}, \mathbf{s}], [\mathbf{z}_n, s_n]) G_n^{-1} \{ \mathbf{f}_n - m_t^{n-1}(\mathbf{z}_n, s_n) \}, \\ C_{xx}^n([\mathbf{Z}, \mathbf{s}], [\mathbf{Z}, \mathbf{s}]) &= C_{xx}^{n-1}([\mathbf{Z}, \mathbf{s}], [\mathbf{Z}, \mathbf{s}]) \\ &\quad - \left\{ \frac{\partial^2}{\partial \mathbf{Z}^2} \int_{a^t}^{\mathbf{s}} C_t^{n-1}([\mathbf{Z}, t], [\mathbf{z}_n, s_n]) dt \right\} G_n^{-1} \left\{ \frac{\partial^2}{\partial \mathbf{Z}^2} \int_{a^t}^{\mathbf{s}} C_t^{n-1}([\mathbf{Z}, t], [\mathbf{z}_n, s_n]) dt \right\}^\top, \\ \frac{\partial^2}{\partial \mathbf{Z}^2} \int_{a^t}^{\mathbf{s}} C_t^n([\mathbf{Z}, t], [\mathbf{Z}, \mathbf{s}]) dt &= \frac{\partial^2}{\partial \mathbf{Z}^2} \int_{a^t}^{\mathbf{s}} C_t^{n-1}([\mathbf{Z}, t], [\mathbf{Z}, \mathbf{s}]) dt \\ &\quad - \left\{ \frac{\partial^2}{\partial \mathbf{Z}^2} \int_{a^t}^{\mathbf{s}} C_t^{n-1}([\mathbf{Z}, t], [\mathbf{z}_n, s_n]) \right\} dt G_n^{-1} C_t^{n-1}([\mathbf{z}_n, s_n], [\mathbf{Z}, \mathbf{s}]), \\ C_t^n([\mathbf{Z}, \mathbf{s}], [\mathbf{Z}, \mathbf{s}]) &= C_t^{n-1}([\mathbf{Z}, \mathbf{s}], [\mathbf{Z}, \mathbf{s}]) - C_t^{n-1}([\mathbf{Z}, \mathbf{s}], [\mathbf{z}_n, s_n]) G_n^{-1} C_t^{n-1}([\mathbf{z}_n, s_n], [\mathbf{Z}, \mathbf{s}]); \end{aligned}$$

if $n < N$ **then**

sample time step ahead realization of the 2nd spatial derivative of the state, $u_{xx}(\mathbf{z}_n, s_{n+1})$ from the predictive distribution,

$$\begin{aligned} p([u_{xx}(z_{1,n}, s_{n+1}), \dots, u_{xx}(z_{M,n}, s_{n+1})] \mid \mathbf{f}_n, \kappa, \Psi_N) \\ = \mathcal{N}([u_{xx}(z_{1,n}, s_{n+1}), \dots, u_{xx}(z_{M,n}, s_{n+1})] \mid m_{xx}^n(\mathbf{z}_n, s_{n+1}), C_{xx}^n([\mathbf{z}_n, s_{n+1}], [\mathbf{z}_n, s_{n+1}])); \end{aligned}$$

and evaluate the PDE model to obtain $\mathbf{f}_{n+1} = \kappa [u_{xx}(z_{1,n+1}, s_{n+1}), \dots, u_{xx}(z_{M,n+1}, s_{n+1})]$

end if

end for

Return $\begin{bmatrix} u(x_{1,1}, t_1) & \cdots & u(x_{X,1}, t_1) \\ \vdots & \vdots & \vdots \\ u(x_{1,1}, t_T) & \cdots & u(x_{X,T}, t_T) \end{bmatrix} \sim \mathcal{GP}(m^N(\mathbf{X}, \mathbf{T}), C^N([\mathbf{X}, \mathbf{T}], [\mathbf{X}, \mathbf{T}]))$, where $\mathbf{X} \subset \mathbf{Z}$ and $\mathbf{T}_{:,1} \subset \mathbf{s}$

The computational cost is proportional to that incurred while using a finite difference numerical approach, which is often large because the number of function evaluations required grows exponentially in the number of spatial dimensions considered. However, as with finite difference methods, this number can be reduced either through implicit or collocation based methods. For that reason, in Section 4.4 a pseudo spectral projection approach is applied to extend the methodology for dealing with much more complex systems.

4.2 Solution multiplicity in a mixed boundary value problem

Mixed boundary value problems introduce challenges for many numerical solvers, which typically rely on optimization and the theory of ODE initial value problems to estimate the unknown initial state, $u(a)$ subject

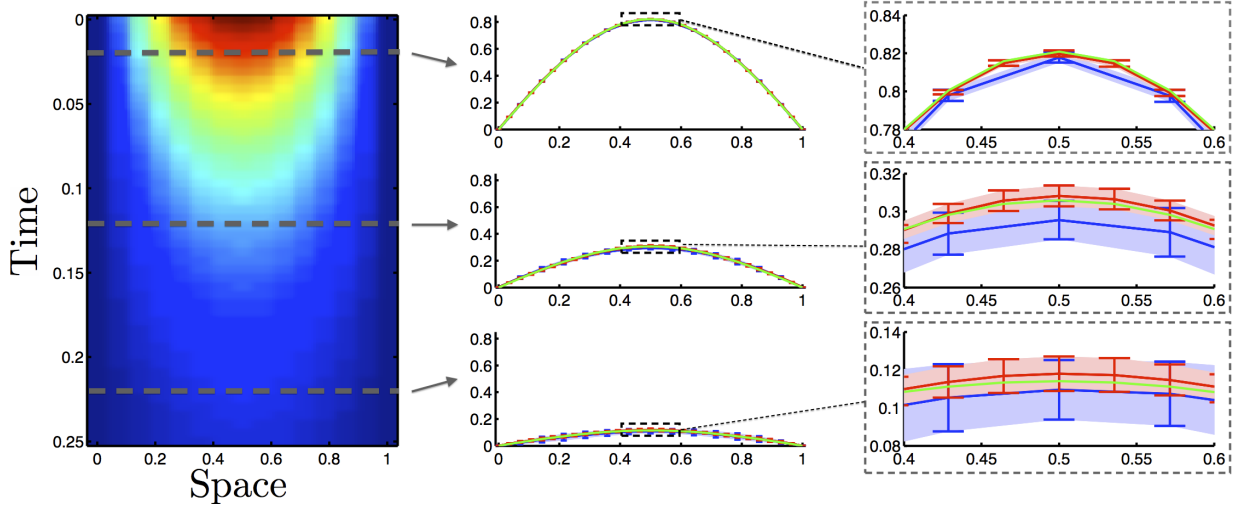


Figure 3: Uncertainty in the solution satisfying the heat equation (8) with $\kappa = 1$, on the domain $\mathcal{D} = [0, 1] \times [0, 0.25]$ using two grid sizes. The coarser mesh (shown in blue) consists of 15 spatial discretization points and 50 time discretization points, the finer mesh consists of 29 spatial discretization points and 100 time discretization points. Spatial posterior predictions are shown at three time points: $t = 0.02$ (top), $t = 0.12$ (middle) and $t = 0.22$ (bottom). The exact solution at each time point is represented by the green line and is assumed a priori unknown. The error bars show the empirical mean and 2 standard deviations computed from 50 simulations.

to the state constraints at either boundary of the domain of integration, $[a, b]$. The optimization over $u(a)$ is performed until the corresponding initial value problem solution satisfies the given boundary condition, $u^*(b)$, to within a user specified tolerance. For expositional simplicity, consider a boundary value problem of the form (5) with one constraint located at each boundary of the domain, namely, $\phi\{v(a), u(b)\} := [v(a), u(b)] - [v^*(a), u^*(b)] = [0, 0]$. The probabilistic framework naturally defines a mismatch tolerance through a predictive distribution by considering the solution as an inference problem over the unspecified initial value, $u(a)$, given its known final value $u^*(b)$. The likelihood therefore defines the mismatch between the boundary value $u(b)$, obtained from the realized probabilistic solution with the exact boundary value, $u^*(b)$, as follows,

$$u^*(b) \mid u(a), v^*(a), \theta, \Psi_N \sim N \left\{ m^{N(u)}(b), C^{N(u)}(b, b) \right\}. \quad (16)$$

where $m^{N(u)}(b)$ and $C^{N(u)}(b, b)$ are the posterior mean and covariance for state u at time point b , obtained via Algorithm 1 at sequential update step N . The posterior distribution of the states over the grid $\mathbf{t} = [t_1, \dots, t_T]$ therefore has density,

$$\begin{aligned} & p\{u(t_1), \dots, u(t_T), v(t_1), \dots, v(t_T), u(a) \mid u^*(b), v^*(a), \theta, \Psi_N\} \\ & \propto p\{u(t_1), \dots, u(t_T), v(t_1), \dots, v(t_T) \mid u(a), u^*(b), v^*(a), \theta, \Psi_N\} \\ & \quad p\{u(a) \mid u^*(b), v^*(a), \theta, \Psi_N\} \pi\{u(a)\}, \end{aligned} \quad (17)$$

which exhibits multimodality over the states when multiple solutions satisfy the mixed boundary value problem, as illustrated in the two leftmost panels of Figure 4. In such cases it may be necessary to use an appropriate Markov chain Monte Carlo scheme, such as parallel tempering (Geyer, 1991), which can quickly identify and explore disjoint regions of high posterior probability. We provide one such implementation of parallel tempering in the Appendix (Algorithm 5).

As a demonstration of modelling the a priori unknown solutions to a mixed boundary value problem probabilistically, we consider a special case the Lane-Emden model, which is used to describe the density, u , of gaseous spherical objects, such as stars, as a function of radius, t , (Shampine, 2003). We rewrite the

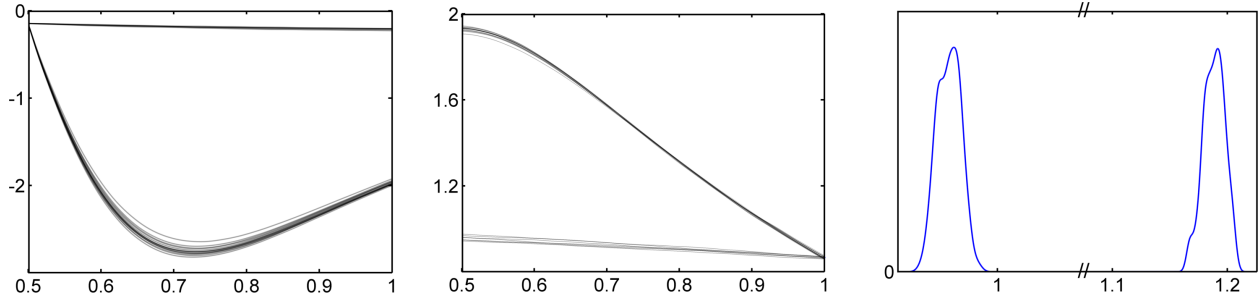


Figure 4: Three dimensions of $L = 100$ realizations from the posterior probability density (17). The states, u and v , evaluated over a fine grid, \mathbf{t} , over the domain, $\mathcal{D} = [\frac{1}{2}, 1]$, are shown in the left and central panels. The marginal un-normalized log posterior density over the unknown initial condition, $u(\frac{1}{2})$, is shown on the right.

canonical second order ODE as a system of a first order equations with a mixed boundary value,

$$\begin{cases} u_t = v, & t \in [\frac{1}{2}, 1], \\ v_t = -2vt^{-1} - u^5, & t \in [\frac{1}{2}, 1], \\ u = \frac{\sqrt{3}}{2}, & t = 1, \\ v = -\frac{288}{2197}, & t = \frac{1}{2}. \end{cases} \quad (18)$$

The unknown initial state $u^*(\frac{1}{2})$ is assigned a diffuse Gaussian prior with mean 1.5 and standard deviation $2|u^*(1) - v^*(\frac{1}{2})|$, which reflects the possibility that multiple solutions may be present over a wide range of initial states. In this example, we chose the squared exponential covariance to model what we expect to be a very smooth solution. The discretization grid consists of 100 equally spaced points. The length-scale is set to twice the discretization grid step size and the prior precision is set to 1. Figure 4 shows posterior samples from Equation (17) and identifies two high density regions in the posterior corresponding to distinct trajectories that approximately satisfy model dynamics. The right side panel of Figure 4 illustrates this multimodality by showing the marginal posterior over the unknown initial state $u(\frac{1}{2})$. These high posterior density regions concentrate as the number of grid points and the prior precision increase, suggesting the potential for defining intermediate target densities for sequential and particle Markov chain Monte Carlo schemes to sample realizations from the posterior distribution over any unknown model parameters within the inverse problem. This example highlights the need for accurately modelling solution uncertainty in a functional manner. The proposed approach allows us to determine the number and location of multiple possible solutions, and account for them probabilistically.

4.3 Forward simulation of a chaotic ODE initial value problem

Chaotic systems arise in modelling a large variety of physical systems, including laser cavities, chemical reactions, fluid motion, crystal growth, weather prediction, and earthquake dynamics (Baker and Gollub, 1996, chapter 7). Extreme sensitivity to small perturbations characterizes chaotic dynamics, where the effect of discretization uncertainty becomes an important contribution to global solution uncertainty. Although the long term behaviour of the system is entrenched in the initial states, the presence of numerical discretization error introduces perturbations which eventually lead to exponential divergence from the exact solution. Consequently, information about initial states rapidly decays as system solution evolves in time. This insight, demonstrated and explained by Berliner (1991) is showcased in the following example.

We consider the classical ‘‘Lorenz63’’ initial value problem (Lorenz, 1963), a seemingly simple three-state ODE model of convective fluid motion induced by a temperature difference between an upper and lower surface. States $u^{(1)}$, $u^{(2)}$ and $u^{(3)}$ are proportional to the intensity of the fluid’s convective motion, the temperature difference between (hot) rising and (cold) descending currents, and the deviation of the vertical

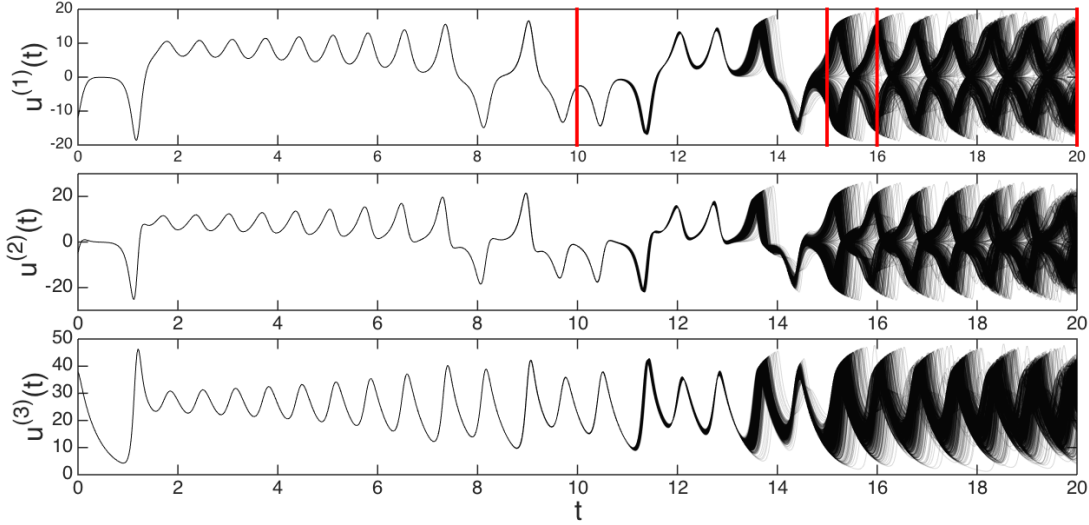


Figure 5: 1000 draws for the Lorenz63 model generated from a probabilistic solver given fixed initial states and model parameters in the chaotic regime. Vertical lines in $u^{(1)}(t)$ correspond to time points chosen for Figure 6a.

temperature profile from linearity respectively. The model describing the time-evolution of their dynamics,

$$\begin{cases} u_t^{(1)} &= -\sigma(u^{(1)} + u^{(2)}), & t \in [0, 20], \\ u_t^{(2)} &= -ru^{(1)} - u^{(2)} - u^{(1)}u^{(3)}, & t \in [0, 20], \\ u_t^{(3)} &= u^{(1)}u^{(2)} - bu^{(3)}, & t \in [0, 20], \\ u &= u^*, & t = 0, \end{cases} \quad (19)$$

depends on dimensionless parameters σ, r and b . The standard choice of $\theta = [\sigma, r, b] = [10, 8/3, 28]$ with initial state $u^*(0) = [-12, -5, 38]$ falls within the chaotic regime. This system has a unique solution whose trajectory lies on a bounded region of the phase space (e.g., Robinson, 2001, pp. 271-272), and is unknown in closed form. The probabilistic algorithm was performed for a discretization grid of size $N = 5001$ equally spaced points on the interval $\mathcal{D} = [0, 20]$. A squared exponential covariance was used, reflecting our assumption of a locally smooth solution, the length scale was set to twice the step size and prior precision was set to N .

A sample of 1000 trajectories generated from the probabilistic solution for this system is shown in Figure 5 given fixed initial condition, $u^*(a)$, model parameters, θ , and hyperparameters, Ψ_N . There is a short time window within which there is negligible uncertainty in the solution, but the accumulation of discretization uncertainty results in rapidly diverging, yet highly structured errors. Figure 6a shows the posterior samples in the 3 state dimensions at 4 different evaluation times while Figure 6b shows density estimates of the samples for $u^{(1)}(t)$. The resulting positions of the trajectories around the attractor highlight marginal multimodality in the model of uncertainty on the state in model (1). These figures highlight the structure of the Lorenz63 sampled trajectories which is not simply defined by a continual widening of the confidence region for each state through the accumulation of additive numerical bounds, but instead exhibits a strong structure that is consistent with the dynamics of the underlying stable attractor.

4.4 Forward simulation for a PDE model of fluid dynamics

We present the following example as a proof of concept illustrating that the probabilistic solver framework developed may be applied reliably and straightforwardly to a high-dimensional dynamical system. The Navier-Stokes system is a fundamental model of fluid dynamics, incorporating laws of conservation of mass, energy and linear momentum, as well as physical properties of an incompressible fluid over some domain given

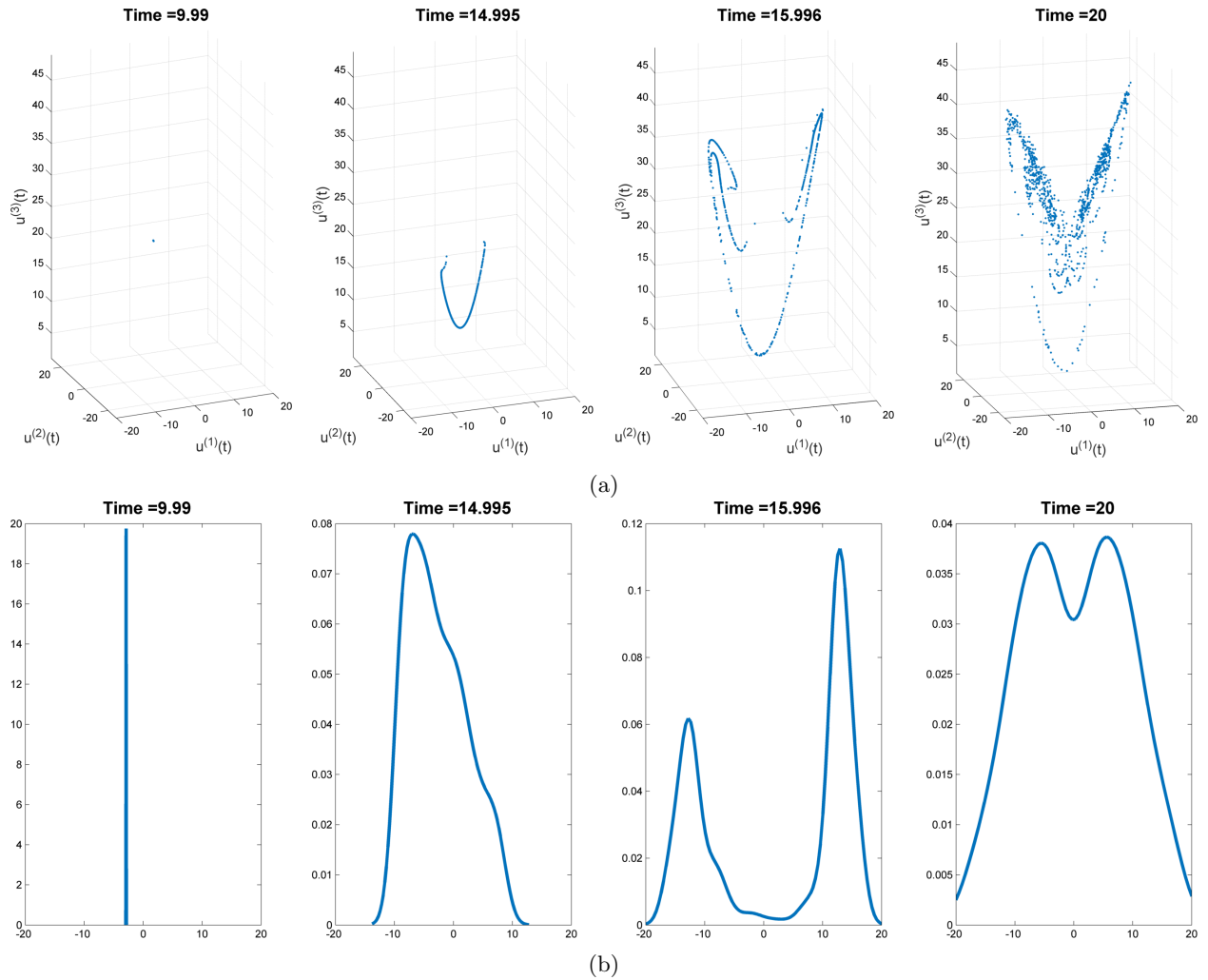


Figure 6: Samples from the probabilistic solver for the Lorenz63 system at 4 time points, shown with vertical lines in Figure 5. (a): Plots of 1000 draws from model (1) for all three states of the Lorenz63 system at fixed time points. (b): Kernel density estimates of the first state's location at fixed time points based on 1000 draws from model (1) for all three states of the Lorenz63 system.

constraints imposed along the boundaries. It is an important component of complex models in oceanography, weather, atmospheric pollution, and glacier movement. Despite its extensive use, the dynamics of Navier-Stokes models are poorly understood even at small time scales, where they can give rise to turbulence.

We consider the Navier-Stokes PDE model for the time evolution of 2 components of the velocity, $u : \mathcal{D} \rightarrow \mathbb{R}^2$, of an incompressible fluid on a torus, $\mathcal{D} = [0, 2\pi) \times [0, 2\pi]$, expressed in spherical coordinates. The Navier-Stokes boundary value problem is defined by:

$$\begin{cases} u_t - \theta \Delta u + (u \cdot \nabla) u &= \mathbf{g} - \nabla \mathbf{p}, & (x, t) \in \mathcal{D} \times [a, b], \\ \nabla \cdot u &= 0, & (x, t) \in \mathcal{D} \times [a, b], \\ \int u^{(j)} dx &= 0, & (x, t) \in \mathcal{D} \times [a, b], j = 1, 2, \\ u &= u^*, & (x, t) \in \mathcal{D} \times \{0\}, \end{cases} \quad (20)$$

where $\Delta := \left[\frac{\partial^2}{\partial x_1^2} + \frac{\partial^2}{\partial x_2^2} \right]$ is the Laplacian operator such that $\Delta u = \left(u_{x_1 x_1}^{(1)} + u_{x_2 x_2}^{(1)}, u_{x_1 x_1}^{(2)} + u_{x_2 x_2}^{(2)} \right)$, and $\nabla := \left[\frac{\partial}{\partial x_1} + \frac{\partial}{\partial x_2} \right]$ is the gradient operator such that $\nabla u = \left(u_{x_1}^{(1)} + u_{x_2}^{(1)}, u_{x_1}^{(2)} + u_{x_2}^{(2)} \right)$. The model is parametrized by the viscosity of the fluid, $\theta \in \mathbb{R}^+$, the pressure function $\mathbf{p} : \mathcal{D} \times [a, b] \rightarrow \mathbb{R}$, and the external time-homogeneous forcing function $\mathbf{g} := 5 \times 10^{-3} \cos \left[\left(\frac{1}{2}, \frac{1}{2} \right) \cdot x \right]$. We further assume periodic boundary conditions, and viscosity $\theta = 10^{-4}$ in the turbulent regime. The exact solution of the Navier-Stokes boundary value problem (20) is not known in closed form.

Often, the quantity of interest is the local spinning motion of the incompressible fluid, called vorticity, which we define as,

$$\varpi = -\nabla \times u,$$

where $\nabla \times u$ represents the rotational curl defined as the cross product of ∇ and u , with positive vorticity corresponding to clockwise rotation. This variable will be used to better visualise the probabilistic solution of the Navier-Stokes system by reducing the two components of velocity to a one dimensional function. We discretize the Navier-Stokes model (20) over a grid of size 128 in each spatial dimension. A pseudo spectral projection in Fourier space yields 16,384 coupled, stiff ODEs with associated constraints. Full details of the pseudo spectral projection are provided on the accompanying website to allow full replication of these results. Figure 7 shows four forward simulated vorticity trajectories (along rows), obtained from two components of velocity governed by the Navier-Stokes equations (20) at four distinct time points (along columns). Slight differences in the state dynamics can be seen at the last time point, where the four trajectories visibly diverge from one another. These differences express the epistemic uncertainty resulting from discretizing the exact but unknown infinite dimensional solution.

5 Exact Bayesian Posterior Inference for the Inverse Problem

We now present a framework for propagating the model discretization uncertainty, characterized in Section 3, through an inverse problem, in which we wish to infer model parameters from measurement data based on the hierarchical model,

$$\begin{aligned} [y(\mathbf{x}, \mathbf{t}) \mid u(\mathbf{x}, \mathbf{t}, \theta), \theta, \Sigma] &\propto \rho [y(\mathbf{x}, \mathbf{t}) - \mathcal{G} \{u(\mathbf{x}, \mathbf{t}, \theta), \theta\}] \\ [u(\mathbf{x}, \mathbf{t}, \theta) \mid \theta, \Psi_N] &\sim \mu^N \\ [\theta, \Psi_N, \Sigma] &\sim \pi(\theta, \Psi_N, \Sigma) \end{aligned}$$

We assume the parameters θ also include any unknown initial conditions or other model components. We describe a Markov chain Monte Carlo procedure that generates a sample from the joint posterior distribution of the state at the data locations $\mathbf{t} = [t_1, \dots, t_T]$ and the unknown parameters θ conditional on noisy observations $y(x_i, t_i) = \mathcal{G} \{u(x_i, t_i), \theta\} + \epsilon(x_i, t_i), 1 \leq i \leq T$ of the states. A situation where states are indirectly observed through a nonlinear transformation \mathcal{G} is described in Section 5.2.

Algorithm 3 generates samples from the posterior distribution in expression (2) by forward model proposals via conditional simulation from Algorithm 1. This proposal step avoids the need to explicitly calculate the intractable marginal density $\int p \{u(x_1, t_1), \dots, u(x_T, t_T), \mathbf{f}_1, \dots, \mathbf{f}_N \mid \theta, \Psi_N\} d\mathbf{f}_1 \cdots d\mathbf{f}_N$, and can be implemented efficiently as described in the Appendix (Section 7.1). Such partially likelihood-free Markov chain

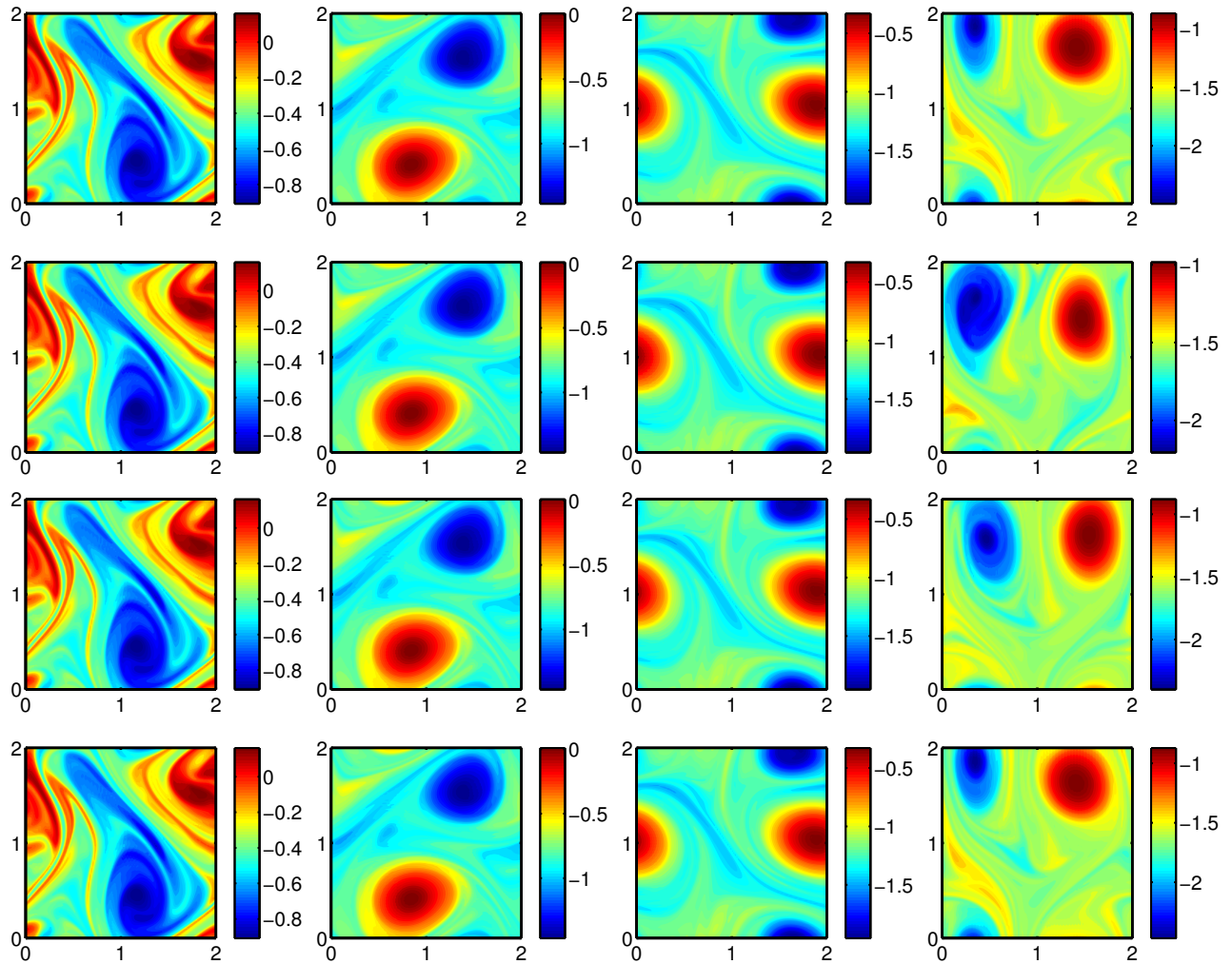


Figure 7: Time evolution of four forward simulated realizations (along rows) of fluid vorticity, governed by the forced Navier-Stokes model (20), over two spatial dimensions: the angle of the inner ring (horizontal axis) and outer ring (vertical axis) of a two dimensional torus. Angles are expressed in radians. Vorticities are evaluated at times $t = [0.2, 0.4, 0.6, 0.8]$ units (along columns).

Monte Carlo implementations (Marjoram et al., 2003) are widely used in the area of inference for stochastic differential equations (see, for example, Golightly and Wilkinson, 2011) for simulating sample paths within the inverse problem.

Algorithm 3 Metropolis-Hastings algorithm to draw L samples from the posterior distribution with density $p\{\theta, u(x_1, t_1), \dots, u(x_T, t_T) \mid y(x_1, t_1), \dots, y(x_T, t_T), \Psi_N, \Sigma\}$ given observations on a transformation \mathcal{G} of the solution of a general differential equation problem with unknown parameter.

Initialize $\theta, \alpha, \lambda \sim \pi(\cdot)$ where π is the prior density;

Use a probabilistic solver (for example Algorithms 1,2,4,5, or 6) to conditionally simulate a vector of realizations, $[u(x_1, t_1), \dots, u(x_T, t_T)]$, of the differential equation model given θ, N and discretization grid \mathbf{S} ;

for $\ell = 1 : L$ **do**

Propose $\theta', \alpha', \lambda' \sim q(\cdot \mid \theta, \alpha, \lambda)$ where q is a proposal density;

Use a probabilistic solver (for example Algorithms 1,2,4,5, or 6) to conditionally simulate a vector of realizations, $[u'(x_1, t_1), \dots, u'(x_T, t_T)]$, of the differential equation model given $\theta', \alpha', \lambda', N$ and discretization grid \mathbf{S} ;

Compute the rejection ratio,

$$\rho = \frac{q(\theta, \alpha, \lambda \mid \theta', \alpha', \lambda')}{q(\theta', \alpha', \lambda' \mid \theta, \alpha, \lambda)} \frac{\pi(\theta, \alpha, \lambda)}{\pi(\theta', \alpha', \lambda')} \frac{p[y(x_1, t_1), \dots, y(x_T, t_T) \mid \mathcal{G}\{u(x_1, t_1, \theta), \theta\}, \dots, \mathcal{G}\{u(x_T, t_T, \theta), \theta\}, \Sigma]}{p[y(x_1, t_1), \dots, y(x_T, t_T) \mid \mathcal{G}\{u'(x_1, t_1, \theta'), \theta'\}, \dots, \mathcal{G}\{u'(x_T, t_T, \theta'), \theta'\}, \Sigma]},$$

if $\min(1, \rho) > U[0, 1]$ **then**

Update $[\theta, \alpha, \lambda] \leftarrow (\theta', \alpha', \lambda')$;

Update $[u(x_1, t_1, \theta), \dots, u(x_T, t_T, \theta)] \leftarrow [u'(x_1, t_1, \theta'), \dots, u'(x_T, t_T, \theta')]$;

end if

Return $[\theta, \alpha, \lambda, u(x_1, t_1, \theta), \dots, u(x_T, t_T, \theta)]$.

end for

As with numerical method based approaches for inference, computation of the forward model is the rate limiting step in Algorithm 3. This is where we can identify some computational savings by exploiting the structure of the probabilistic solver. For example, an equivalent formulation of the forward simulation algorithm (Chkrebtii, 2013) requires less computational time to draw M additional joint auxiliary and forward model realizations compared to repeating the full algorithm. This fact can be exploited within the inverse problem by using an ensemble Markov chain Monte Carlo sampling scheme, as proposed by Neal (2011), that allows sampling from mixture distributions for which multiple realizations can be quickly computed.

We now have all the components to take a fully Bayesian approach for quantifying uncertainty on differential equation models of natural and physical systems. The remainder of this section applies the inverse problem formulation to PDE and DIFP models.

5.1 Inferring conductivity in a parabolic PDE boundary value problem

We now present an illustrative example of inference using the heat equation model (8). Although we consider this simple system for expositional clarity, the characterization of spatial uncertainty is vital for more complex models, in cases where there are computational constraints limiting the number of system evaluations that may be performed. We can see the effect of such discretization uncertainty by performing posterior inference for the parameter κ given data simulated from an exact solution with $\kappa = 1$ and zero mean Gaussian error with standard deviation of 0.005. Figure 8 shows the posterior distribution over κ obtained by using both a deterministic “forward in time, centred in space” (FTCS) finite difference solver and a probabilistic solver under a variety of discretization grids. Note the change in the scale as the mesh is refined and the posterior variance decreases. The use of a deterministic solver illustrates the problem of inferential bias

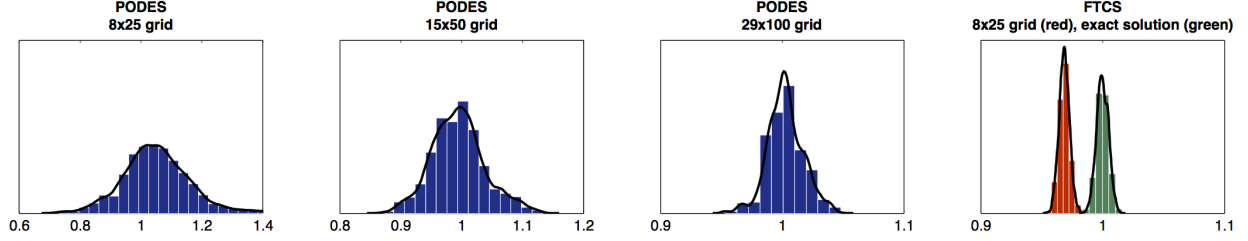


Figure 8: Posterior densities for the conductivity parameter κ in the heat equation model (8) on the domain $\mathcal{D} = [0, 1] \times [0, 0.25]$ conditional on simulated data generated over a grid of 8 spatial and 25 temporal discretization points from the exact solution with $\kappa = 1$. Inference is based on the probabilistic differential equation solver (PODES) using three grid sizes: a coarse mesh consisting of 8 spatial and 25 temporal discretization points (far left), a finer mesh consisting of 15 spatial and 50 temporal discretization points (second from left), and a further refined mesh consisting of 29 spatial and 100 temporal discretization points (second from right). For comparison, we provide the posterior density based on a deterministic forward in time, centred in space (FTCS) integration scheme and the posterior density based on the exact solution (far right, red and green respectively).

and overconfident posterior variance that may occur if discretization uncertainty is not taken into account and too coarse a grid is employed. If the discretization is not fine enough, the approximate posterior assigns negligible probability mass to the true value of κ , in contrast to the unbiased posterior obtained when employing the exact solution for inference. In this illustrative setting, the use of a probabilistic solver propagates discretization uncertainty in the solution through to the posterior distribution over the parameters. By using a probabilistic solver with the same coarsely discretized grid in this example, the low variance yet highly biased result of the deterministic numerical approach is exchanged for a higher variance density that is approximately centred on the true value of κ .

5.2 Inference on a delay initial function model of cellular biochemical dynamics

In addition to modelling discretization uncertainty in a structured, functional way, the probabilistic framework provides a straightforward means for the uncertainty in the initial function to be incorporated through the forward simulation. Indeed, the initial function $\phi(t)$ may itself only be available at a finite number of nodes. The probabilistic approach quantifies the uncertainty associated with the estimation of $\phi(t)$ and propagates it recursively through the states. Even when $\phi(t)$ is fully specified in advance, the dependence of the current state on previously estimated states impacts the accuracy of the numerical solution using standard solvers, even over the short term. In the following example we account for the uncertainty associated with current and delayed estimates of system states, and include these potential sources of bias in the estimation of model parameters. The probabilistic approach for forward simulation of delay initial function problems is described in Algorithm 6 in Appendix 7.1. The associated algorithm describes the extension of the updating strategy to accommodate current and lagged auxiliary variable information.

The JAK-STAT mechanism describes a series of reversible biochemical reactions of STAT-5 transcription factors in response to binding of the Erythropoietin (Epo) hormone to cell surface receptors (Pellegrini and Dusanter-Fourt, 1997). After gene activation occurs within the nucleus, the transcription factors revert to their initial state, returning to the cytoplasm to be used in the next activation cycle. This last stage is not well understood and is proxied in the model by the unknown time delay τ . The model for this mechanism describes changes in 4 reaction states of STAT-5 through the nonlinear DIFP,

$$\begin{cases} u_t^{(1)}(t) = -k_1 u^{(1)}(t) \text{Epo}R_A(t) + 2k_4 u^{(4)}(t - \tau), & t \in [0, 60], \\ u_t^{(2)}(t) = k_1 u^{(1)}(t) \text{Epo}R_A(t) - k_2 u^{(2)2}(t), & t \in [0, 60], \\ u_t^{(3)}(t) = -k_3 u^{(3)}(t) + \frac{1}{2} k_2 u^{(2)2}(t), & t \in [0, 60], \\ u_t^{(4)}(t) = k_3 u^{(3)}(t) - k_4 u^{(4)}(t - \tau), & t \in [0, 60], \\ u(t) = \phi(t), & t \in [-\tau, 0]. \end{cases} \quad (21)$$

The initial function components $\phi^{(2)}(t) = \phi^{(3)}(t) = \phi^{(4)}(t)$ are everywhere zero, while the constant initial function $\phi^{(1)}(t)$ is unknown.

The states for this system cannot be measured directly, but are observed through a nonlinear transformation, $\mathcal{G} : \mathbb{R}^3 \times \Theta \rightarrow \mathbb{R}^4$, defined as,

$$\mathcal{G} \{u(t), \theta\} = \begin{cases} k_5 \{u^{(2)}(t) + 2u^{(3)}(t)\} \\ k_6 \{u^{(1)}(t) + u^{(2)}(t) + 2u^{(3)}(t)\} \\ u^{(1)}(t) \\ u^{(3)}(t) \{u^{(2)}(t) + u^{(3)}(t)\}^{-1} \end{cases} \quad (22)$$

and parameterized by the unknown scaling factors k_5 and k_6 . The indirect measurements of the states,

$$y^{(j)}(t_{j,i}) = \mathcal{G}^j \{u(t_{j,i}), \theta\} + \varepsilon^{(j)}(t_{j,i}), \quad 1 \leq i \leq T_j, 1 \leq j \leq 4.$$

are assumed contaminated with additive zero mean Gaussian noise, $\{\varepsilon^{(j)}(t_{j,i})\}_{1 \leq i \leq T_j, 1 \leq j \leq 4}$, with experimentally determined standard deviations. Analysis is based on experimental data measured at the locations, $\{t_{j,i}\}_{1 \leq i \leq T_j, 1 \leq j \leq 4}$, from Swameye et al. (2003), which consists of 16 measurements for the first two states of the observation process. Following Raue et al. (2009) an additional artificial data point for each of the third and fourth observation process states is included to deal with lack of parameter identifiability for this system. The forcing function, $\text{Epo}R_A : [0, 60] \rightarrow \mathbb{R}^+$, is not known, but measured at 16 discrete time points $t_{EPO,1}, \dots, t_{EPO,16}$. As per Raue et al. (2009), we assume that Epo concentrations are measured without error. We further assume that this function shares the same smoothness as the solution state (piecewise linear first derivative). The full conditional distribution of the forcing function is given by a GP interpolation of the observations. Forward inference for this model will be used within the statistical inverse problem of recovering unknown parameters and first initial state, $\theta = [k_1, \dots, k_6, \tau, u^{(1)}(0)]$, from experimental data.

We demonstrate probabilistic inference for state trajectories and parameters of the challenging 4 state delay initial function model (21) describing the dynamics of the JAK-STAT cellular signal transduction pathway (Raue et al., 2009). There have been several analyses of the JAK-STAT pathway mechanism based on this data (e.g., Campbell and Chkrebti, 2013; Raue et al., 2009; Schmidl et al., 2013; Swameye et al., 2003). Despite the variety of modelling assumptions considered by different authors, as well as distinct inference approaches, some interesting common features have been identified that motivate the explicit modelling of discretization uncertainty for this application. Firstly, the inaccuracy and computational constraints of numerical techniques required to solve the system equations have led some authors to resort to coarse ODE approximations or even approximating the numerical solution via Generalised Smoothing methods. This motivates a formal analysis of the structure and propagation of discretization error through the inverse problem. A further issue is that the model (21) and its variants are likely misspecified, a type of uncertainty that must be uncoupled from discretization effects in order to be studied. Indeed, the above cited analyses conclude that the model is not flexible enough to fit the available data, however it is not clear how much of this misfit is due to model discrepancy, and how much may be attributed to discretization error.

Parameters	Prior
τ	χ_6^2
$\lambda_i, 1 \leq i \leq 4$	χ_1^2
$\alpha_i + 100, 1 \leq i \leq 4$	$\text{Log-}\mathcal{N}(10, 1)$
$k_i, 1 \leq i \leq 6$	$\text{Exp}(1)$
$u^{(1)}(0)$	$N(y^{(3)}(0), 40^2)$

Table 1: Priors on the model and auxiliary parameters.

Priors are defined in Table 1. Markov chain Monte Carlo can be used to (See Appendix Section 7.1 Algorithm 7) to obtain samples from the posterior distribution of the model parameters, $\theta = [k_1, \dots, k_6, \tau, u^{(1)}(0)]$, solution states, $\{u(t_{j,i}, \theta)\}_{1 \leq i \leq T_j, 1 \leq j \leq 4}$, and auxiliary variables, α and λ given the data $\{y(t_{j,i})\}_{1 \leq i \leq T_j, 1 \leq j \leq 4}$. In order to construct a Markov chain that efficiently traverses the parameter space of this multimodal posterior distribution, we employed a parallel tempering sampler (Geyer, 1991) with 10 parallel chains along a uniformly spaced temperature profile over the interval $[0.5, 1]$ as outlined in Appendix Section 7.1 Algorithm

8. Each realization from the probability model for the unknown solution of the JAK-STAT delay initial function model was generated using Algorithm 6 under an equally spaced discretization grid of size $N = 500$, and the uniform covariance kernel $R_\lambda(t_j, t_k) = 1_{(t_j - \lambda, t_j + \lambda)}(t_k)$.

We obtained two groups of posterior samples, each of size 50,000. Within chain convergence was assessed by testing for equality of means between disjoint iteration intervals of the chain (Geweke 1992). Between chain convergence was similarly assessed. Additionally we ensured that the acceptance rate fell roughly within the accepted range of 18%–28% for each of the two parameter blocks, and that the total acceptance rate for moves between any two chains remained roughly within 5%–15%.

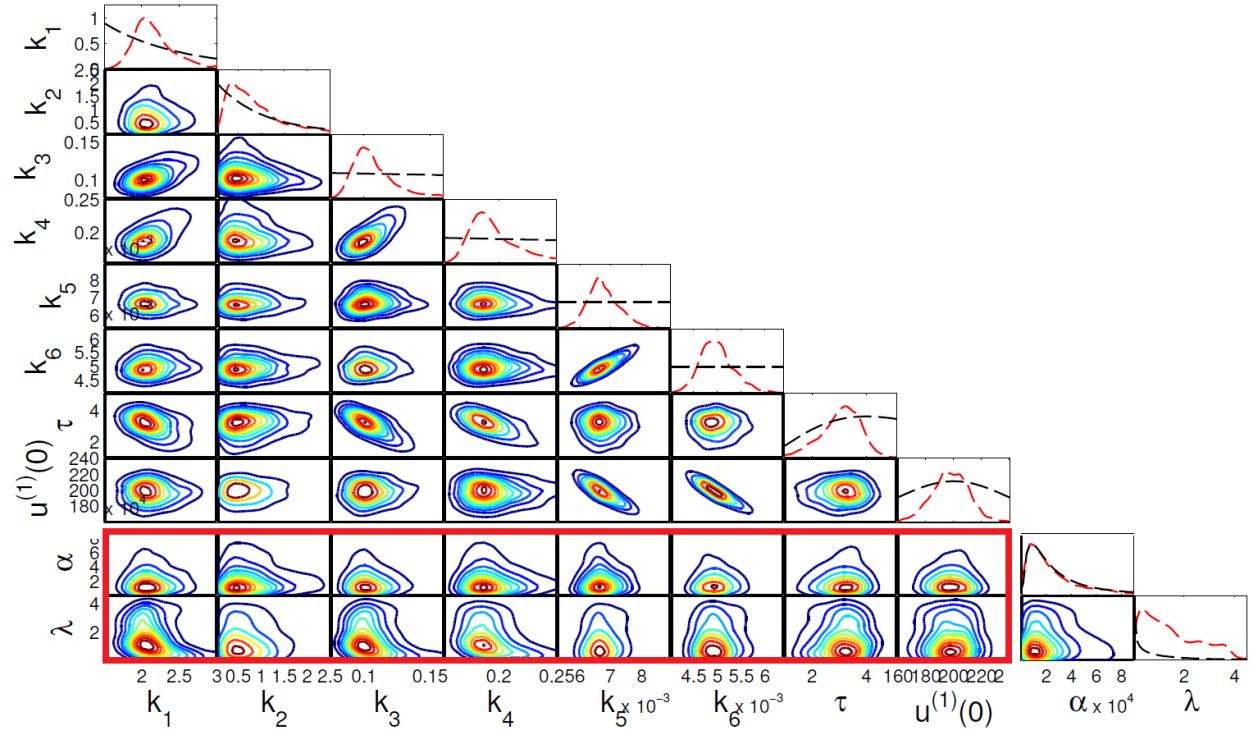


Figure 9: 50,000 posterior samples of the model parameters using a probabilistic solver with a grid of size 500, generated using parallel tempering algorithm 8 with ten chains. Prior probability densities are shown in black. Marginal correlations between hyperparameters defining the solver and model parameters are outlined in red.

Correlation plots and kernel density estimates with priors for the marginal parameter posteriors are shown in Figure 9. All parameters with the exception of the prior precision α are identified by the data, including the rate parameter k_2 which appears to be only weakly identified. We observe strong correlations between parameters, consistent with previous studies on this system. For example, there is strong correlation among the scaling parameters k_5, k_6 and the initial first state $u^{(1)}(0)$. Interestingly, there appears to be a relationship between the probabilistic solver’s length-scale λ and the first, third and fourth reaction rates. Furthermore, this relationship has a nonlinear structure, where the highest parameter density region seems to change with length scale implying strong sensitivity to the solver specifications. The length-scale is the probabilistic analogue, under a bounded covariance, of the step number in a numerical method. However, in analyses based on numerical integration, the choice of a numerical technique effectively fixes this parameter at an arbitrary value that is chosen a priori. The result here suggests that for this problem, the inferred parameter values are highly and nonlinearly dependent on the choice of the numerical method used.

A sample from the marginal posterior of state trajectories and the corresponding observation process are shown in Figure 10. The error bars on the data points show two standard deviations of the measurement error from Swameye et al. (2003). It is immediately clear that our model, which incorporates discretization uncertainty in the forward problem, still does not fully capture the dynamics of the observed data. This

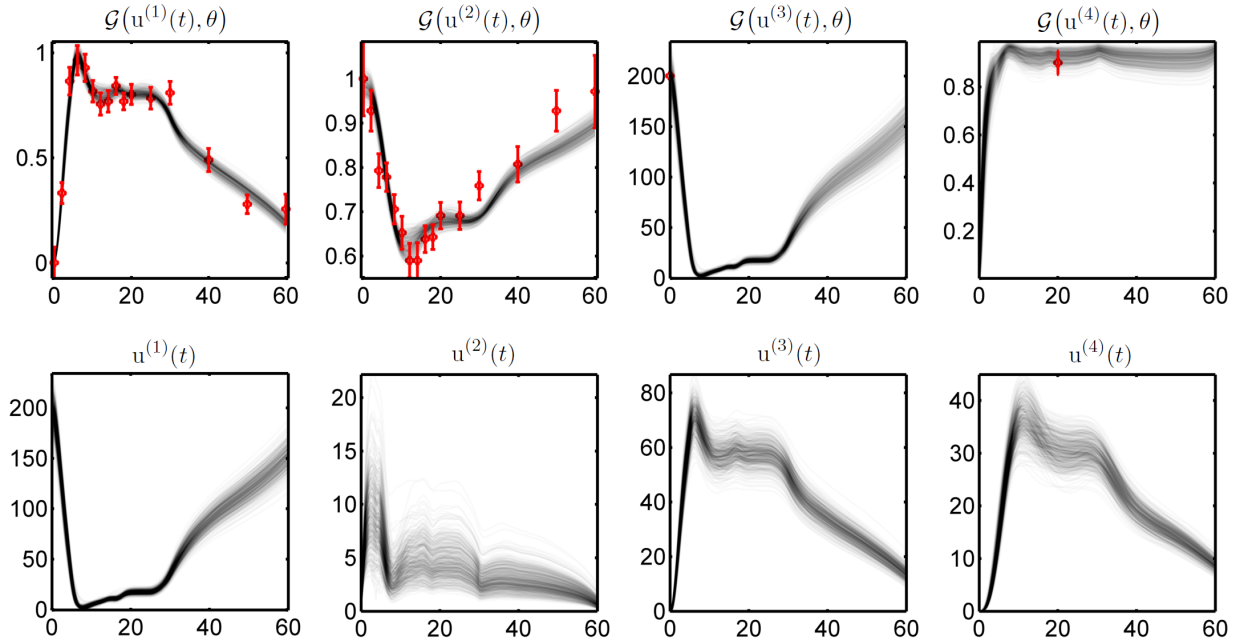


Figure 10: Experimental data (red points) and error bars showing two standard deviations of the measurement error from Swameye et al. (2003). Top row: sample paths (grey lines) of the observation processes obtained by transforming a sample from the marginal posterior distribution of the states (bottom row) by the observation function (22).

systematic lack of fit suggests the existence of model discrepancy beyond that described by discretization uncertainty.

6 Discussion

This paper presents a general Bayesian formalism for characterizing the structure of discretization uncertainty in the solution of differential equations. Discretization uncertainty for dynamical systems may be naturally described in terms of degrees of belief, an idea first formulated by Skilling (1991) and O’Hagan (1992). A Bayesian function estimation approach offers a way of defining and updating our beliefs about probable model trajectories conditional on interrogation of the differential equation model. The resulting uncertainty over the solution can then be propagated through the inferential procedure by defining the probabilistic solver as an additional layer in the Bayesian posterior hierarchy. As such, the proposed formulation is a radical departure from the existing practice of constructing an approximate statistical error model for the data using numerical techniques, and prompts discussion of the emerging field of probabilistic numerics.

The more general goal of studying other sources of model uncertainty requires first understanding how much is known about the dynamics of the proposed model and how that information changes with time, space, and parameter settings. Fundamentally, the probabilistic approach we advocate defines a formal trade-off between solution accuracy and the size of the inverse problem, by choice of discretization grid size. This relationship has been of deep interest in the uncertainty quantification community (see, for example, Arridge et al., 2006; Kaipio et al., 2004) and our approach offers a way of resolving the individual contributions to overall uncertainty from discretization, model misspecification (in the sense of Kennedy and O’Hagan, 2001), and Monte Carlo error within the probabilistic framework.

The area of probabilistic numerics is an emerging field at the intersections of Statistics with Applied Mathematics, Numerical Analysis, and Computer Science, and we hope that this paper will provide a starting point for further work in this area. In particular, while the proposed approach is computationally competitive with other first order methods, it will be important for higher order convergent probabilistic methods to

be developed in the future, such that these approaches may compete with the state-of-the-art deterministic solvers that have resulted from over a century of research into numerical methods. The idea of updating a prior distribution over possible solutions conditional on sequential model interrogations may be expanded by generating new sampling schemes that complement the basic one step ahead choice studied in detail in this contribution. One strategy may be the development of a sampling scheme based on $K > 1$ model interrogations, sampled at intermediate values between discretization grid points. Many traditional higher order numerical solvers (e.g. explicit fourth order Runge-Kutta) use such a carefully constructed weighted average of model interrogations at intermediate values between discretization grid points. Therefore the updating scheme based on multiple samples sequentially placed between grid points provides a clear example where a numerical method can be interpreted in the context of a general probabilistic framework (Schober et al., 2014). It is not surprising that a self-consistent modelling approach should have some similarities to numerical methods whose form has been chosen for their convergence properties. From the perspective presented in this paper, rather than emulate numerical solvers, quadrature is automatically provided by the Gaussian process integration that occurs at each step of Algorithm 1. If the solution smoothness is correctly specified a-priori via the covariance structure, then the chosen covariance structure will naturally yield an appropriate quadrature rule.

Modelling uncertainty about an exact but unknown solution probabilistically may be viewed as providing both an estimate of the exact solution and its associated functional error analysis. Although proportionally scalable, uncertainty quantification methods are naturally more expensive than deterministic numerical approximations obtained without their associated error analyses. Therefore, the question arises of when one may be justified in using a deterministic numerical approximation instead of a probabilistic solver to define the error model for a particular problem. As expected, low dimensional, stable systems, without any topological restrictions on the solution may not suffer from significant discretization effects at a reasonably fine discretization grid. However, it is often difficult to determine a priori whether this stability will persist across the entire parameter space. An example is illustrated by the JAK-STAT case study, where the relationships between model parameters and solver specifications (reflecting changes in the system dynamics) may introduce bias in the estimation of parameters to which the trajectory is highly sensitive. If model uncertainty is indeed negligible and comparable over all parameter settings, sampled trajectories obtained via the probabilistic method will have little variability around the exact solution. If, however, the chosen discretization grid becomes too coarse with respect to the rate of change of system dynamics over some subset of the input space, the uncertainty associated with the model error will be accounted and propagated. For this reason, it may be prudent to adopt a probabilistic approach if one cannot be reasonably certain of negligible and comparable discretization error across all parameter settings.

The probabilistic framework can be used to optimize computation. For a given discretization grid size, a natural question is how we can arrange the grid on the domain in such a way that the resulting approximation is as close as possible in terms of some specified criterion. Most commercially available numerical differential equation solvers select the step length of the discretization grid sequentially. Controlling the local error by choice of the distance between neighbouring grid locations is called *adaptive step size selection*. For example, in the simplest cases, this is accomplished by evaluating the local truncation error at each step and halving the step size if this exceeds an error tolerance that is pre-specified by the user (the process may be repeated several times per step until an appropriate local truncation error is achieved). In a similar way to local truncation error, a predictive probability model of discretization uncertainty may be used to guide sequential mesh refinement and indeed mesh design for complex dynamical systems. Optimising a chosen design criterion would yield the desired discretization grid, as suggested by Skilling (1991). Some initial work in this direction has been conducted in Chkrebtii (2013), where it is shown that the natural Kullback-Leibler divergence criterion may be successfully used to adaptively choose the discretization grid in a probabilistic manner.

Prior specifications and the error model structure may be used to rule out un-physical trajectories that would otherwise arise from a numerical approximation. In numerical analysis, specialized techniques are developed and shown to satisfy certain properties or constraints for a given class of differential equations. A probabilistic framework would permit imposing such constraints in a more flexible and general way. Smoothness constraints on the solution may be incorporated through the prior, and anisotropy in the trajectory may be incorporated at each step through the covariance and the structure of the error model. Although in such general cases it may no longer be possible to obtain closed form representations of the sequential

prior updates, an additional layer of Monte Carlo sampling may be used to marginalise over the realizations required to interrogate the differential equation model.

Inference and prediction for computer experiments (Sacks et al., 1989) is based on a model of the response surface, or emulator, constructed from numerical solutions of prohibitively expensive large-scale system models over a small subset of parameter regimes. Currently, numerical uncertainty is largely ignored when emulating a computer model, although it is informally incorporated through a covariance nugget (see, for example, Gramacy and Lee, 2012) whose magnitude is often chosen heuristically. Adopting a probabilistic approach on a large scale will have practical implications in this area by permitting relaxation of the error-free assumption adopted when modelling computer code output, leading to more realistic and flexible emulators.

The functional model updating structure we have proposed opens up the research of probabilistic numerical analysis. For example, many models for uncertainty such as in weather prediction are performed by perturbing initial conditions and examining the output, however probabilistic solvers can be used with fixed initial conditions and grid discretization to return a distribution of model solutions accounting for numerical uncertainty. Additionally, although numerical approximations of chaotic systems are inherently deterministic, qualitative dynamics (of models such as Lorez63) are often studied statistically by introducing artificial perturbations on the numerical trajectory. For example, the rate of exponential growth (the *Lya-punov exponent*) between nearby trajectories can be estimated via Monte Carlo by introducing small changes to the numerical trajectory over a grid defined along the domain. Our proposed approach explicitly models discretization uncertainty and therefore offer an alternative to such artificial perturbations, thus opening new avenues for exploring uncertainty in the system’s qualitative features.

The developments of our formulation lie at the frontier of research in uncertainty quantification, dealing with massive nonlinear models, exhibiting complex or even chaotic dynamics, and strong spatial-geometric effects (e.g. subsurface flow models). Even solving such systems approximately is a problem that is still at the edge of current research in numerical analysis.

Acknowledgements

We would like to thank Tan Bui, Simon Byrne, Mike Dowd, Des Higham, Richard Lockhart, Youssef Marzouk, Giovanni Petris, Daniel Simpson, John Skilling, Andrew Stuart, and Wen Zhou for their invaluable comments and suggestions.

We would also like to acknowledge the funding agencies that have supported this research. Natural Sciences and Engineering Research Council of Canada supported O.A. Chkrebtii (2010:389148) and D. A. Campbell (RGPIN04040-2014). M.A. Girolami is supported by the UK Engineering and Physical Sciences Council (EPSRC) via the Established Career Research Fellowship EP/J016934/1 and the Programme Grant Enabling Quantification of Uncertainty for Large-Scale Inverse Problems, EP/K034154/1, <http://www.warwick.ac.uk/equip>. He also gratefully acknowledges support from a Royal Society Wolfson Research Merit Award. B. Calderhead gratefully acknowledges his previous Research Fellowship through the 2020 Science programme, funded by EPSRC grant number EP/I017909/1 and supported by Microsoft Research, as well as support in part by EPSRC Mathematics Platform grant EP/I019111/1.

References

- Arridge, S. R., J. P. Kaipio, V. Kolehmainen, M. Schweiger, E. Somersalo, T. Tarvainen, and M. Vauhkonen (2006). Approximation errors and model reduction with an application in optical diffusion tomography. *Inverse Problems* 22(1), 175–195.
- Baker, G. and J. Gollub (1996). *Chaotic Dynamics: an Introduction*. Cambridge University Press.
- Bellen, A. and M. Zennaro (2003). *Numerical Methods for Delay Differential Equations*. Clarendon Press.
- Berliner, L. M. (1991). Likelihood and Bayesian prediction of chaotic systems. *Journal of the American Statistical Association* 86(416), 938–952.

- Bock, H. G. (1983). Recent advances in parameter identification techniques for ODE. In P. Deuffhard and E. Harrier (Eds.), *Numerical treatment of inverse problems in differential and integral equations*, pp. 95–121. Birkhuser.
- Brunel, N. J. (2008). Parameter estimation of ODEs via nonparametric estimators. *Electronic Journal of Statistics* 2, 1242–1267.
- Butcher, J. (2008). *Numerical Methods for Ordinary Differential Equations*. John Wiley and Sons Ltd.
- Calderhead, B. and M. Girolami (2011). Statistical analysis of nonlinear dynamical systems using differential geometric sampling methods. *Interface Focus* 1(6), 821–835.
- Campbell, D. and R. J. Steele (2011). Smooth functional tempering for nonlinear differential equation models. *Statistics and Computing* 22, 429–443.
- Campbell, D. A. and O. Chkrebtii (2013). Maximum profile likelihood estimation of differential equation parameters through model based smoothing state estimates. *Mathematical Biosciences* 246, 283–292.
- Chkrebtii, O. (2013). *Probabilistic solution of differential equations for Bayesian uncertainty quantification and inference*. Ph. D. thesis, Simon Fraser University.
- Coddington, A. and N. Levinson (1955). *Theory of ordinary differential equations*. International series in pure and applied mathematics. McGraw-Hill.
- Dowd, M. (2007). Bayesian statistical data assimilation for ecosystem models using Markov Chain Monte Carlo. *Journal of Marine Systems* 68(3-4), 439–456.
- Geyer, C. (1991). Markov chain Monte Carlo maximum likelihood. In *Computing Science and Statistics, Proceedings of the 23rd Symposium on the Interface*, 156. American Statistical Association.
- Ghanem, R. and P. Spanos (2003). *Stochastic finite elements: a spectral approach*. Springer-Verlag.
- Golightly, A. and D. J. Wilkinson (2011). Bayesian parameter inference for stochastic biochemical network models using particle Markov chain Monte Carlo. *Interface Focus* 1, 807–820.
- Gramacy, R. and H. Lee (2012). Cases for the nugget in modeling computer experiments. *Statistics and Computing* 22, 713–722.
- Gugushvili, S. and C. A. Klaassen (2012). Root n-consistent parameter estimation for systems of ordinary differential equations: bypassing numerical integration via smoothing. *Bernoulli* 18, 1061–1098.
- Higdon, D. (1998). A process-convolution approach to modeling temperatures in the north Atlantic ocean. *Journal of Environmental and Ecological Statistics* 5, 173–190.
- Higdon, D. (2002). *Space and space-time modeling using process convolutions*, pp. 37–54. London, UK: Springer Verlag.
- Huttunen, J. M. J. and J. P. Kaipio (2007). Approximation error analysis in nonlinear state estimation with an application to state-space identification. *Inverse Problems* 23(5), 2141.
- Ionides, E., C. Bretó, and A. King (2006). Inference for nonlinear dynamical systems. *Proceedings of the National Academy of Sciences of the United States of America* 103(49), 18438–18443.
- Kaipio, J. and E. Somersalo (2007). Statistical inverse problems: Discretization, model reduction and inverse crimes. *Journal of Computational and Applied Mathematics* 198, 493–504.
- Kaipio, J. P., A. Seppanen, E. Somersalo, and H. Haario (2004). Posterior covariance related optimal current patterns in electrical impedance tomography. *Inverse Problems* 20(3), 919.
- Keller, H. B. (1968). *Numerical Methods for Two-point Boundary-value Problems*. Blaisdell Publishing Company.

- Kennedy, M. C. and A. O’Hagan (2001). Bayesian calibration of computer models. *Journal of the Royal Statistical Society B* 63(3), 425–464.
- Kim, J.-h., T. Abel, O. Agertz, G. L. Bryan, D. Ceverino, C. Christensen, C. Conroy, A. Dekel, N. Y. Gnedin, N. J. Goldbaum, J. Guedes, O. Hahn, A. Hobbs, P. F. Hopkins, C. B. Hummels, F. Iannuzzi, D. Keres, A. Klypin, A. V. Kravtsov, M. Krumholz, Mark R. and Kuhlen, S. N. Leitner, P. Madau, L. Mayer, C. E. Moody, K. Nagamine, M. L. Norman, J. Onorbe, B. W. O’Shea, A. Pillepich, J. R. Primack, T. Quinn, J. I. Read, B. E. Robertson, M. Rocha, D. H. Rudd, S. Shen, B. D. Smith, A. S. Szalay, R. Teyssier, R. Thompson, K. Todoroki, M. J. Turk, J. W. Wadsley, J. H. Wise, A. Zolotov, and for the AGORA Collaboration²⁹ (2014). The agora high-resolution galaxy simulations comparison project. *The Astrophysical Journal Supplement Series* 210(1), 14.
- Leone, F. C., L. S. Nelson, and R. B. Nottingham (1961). The folded normal distribution. *Technometrics* 3, 543–550.
- Liang, H. and H. Wu (2008). Parameter estimation for differential equation models using a framework of measurement error in regression models. *Journal of the American Statistical Association* 103(484), 1570–1583.
- Lorenz, E. N. (1963). Deterministic nonperiodic flow. *Journal of the Atmospheric Sciences* 20, 130–141.
- Marjoram, P., J. Molitor, V. Plagnol, and S. Tavaré (2003). Markov chain Monte Carlo without likelihoods. *Proceedings of the National Academy of Sciences* 100(26), 15324–15328.
- Marzouk, Y. and H. Najm (2009). Dimensionality reduction and polynomial chaos acceleration of Bayesian inference in inverse problems. *Journal of Computational Physics* 228(6), 1862–1902.
- Marzouk, Y., H. Najm, and L. Rahn (2007). Stochastic spectral methods for efficient Bayesian solution of inverse problems. *Journal of Computational Physics* 224(2), 560–586.
- Neal, R. M. (2011). MCMC using ensembles of states for problems with fast and slow variables such as Gaussian process regression. *arXiv:1101.0387*.
- Oberkampf, W. and C. Roy (2010). *Verification and Validation in Scientific Computing*. Cambridge University Press.
- O’Hagan, A. O. (1992). Some Bayesian numerical analysis. *Bayesian Statistics* 4, 345–363.
- Oliver, T., N. Malaya, R. Ulerich, and R. Moser (2014). Estimating uncertainties in statistics computed from direct numerical simulation. *Physics of Fluids* (26).
- Oliver, T. and R. Moser (2011). Bayesian uncertainty quantification applied to RANS turbulence models. *13th European Turbulence Conference* (318).
- Pellegrini, S. and I. Dusanter-Fourt (1997). The structure, regulation and function of the janus kinases (JAKs) and the signal transducers and activators of transcription (STATs). *European Journal of Biochemistry* 248(3), 615–633.
- Polyanin, A. D. and V. F. Zaitsev (2004). *Handbook of Nonlinear Partial Differential Equations*. Chapman and Hall, CRC Press.
- Ramsay, J., G. Hooker, D. Campbell, and J. Cao (2007). Parameter estimation for differential equations: a generalized smoothing approach. *Journal of the Royal Statistical Society B* 69, 741–796.
- Rasmussen, C. E. and C. K. I. Williams (2006). *Gaussian Processes for Machine Learning*. Cambridge, Massachusetts: MIT Press.
- Raue, A., C. Kreutz, T. Maiwald, J. Bachmann, M. Schilling, U. Klingmüller, and J. Timmer (2009). Structural and practical identifiability analysis of partially observed dynamical models by exploiting the profile likelihood. *Bioinformatics* 25, 1923–1929.

- Robinson, J. (2001). *Infinite-Dimensional Dynamical Systems: An Introduction to Dissipative Parabolic PDEs and the Theory of Global Attractors*. Cambridge Texts in Applied Mathematics. Cambridge University Press.
- Sacks, J., W. J. Welch, T. J. Mitchell, and H. P. Wynn (1989). Design and analysis of computer experiments. *Statistical Science* 4(4), 409–423.
- Schmidl, D., C. Czado, S. Hug, and F. J. Theis (2013). A vine-copula based adaptive MCMC sampler for efficient inference of dynamical systems. *Bayesian Analysis* 8(1), 1–22.
- Schober, M., D. K. Duvenaud, and P. Hennig (2014). Probabilistic ODE solvers with Runge-Kutta means. In Z. Ghahramani, M. Welling, C. Cortes, N. Lawrence, and K. Weinberger (Eds.), *Advances in Neural Information Processing Systems 27*, pp. 739–747. Curran Associates, Inc.
- Shampine, L. (2003). Singular boundary value problems for ODEs. *Applied Mathematics and Computation* 138, 99 – 112.
- Skilling, J. (1991). *Bayesian Solution of Ordinary Differential Equations*, pp. 23–37. Seattle: Kluwer Academic Publishers.
- Stuart, A. M. (2010). Inverse problems: A Bayesian perspective. *Acta Numerica* 19, 451–559.
- Swameye, I., T. Muller, J. Timmer, O. Sandra, and U. Klingmuller (2003). Identification of nucleocytoplasmic cycling as a remote sensor in cellular signaling by databased modeling. *Proceedings of the National Academy of Sciences* 100, 1028–1033.
- Xue, H., H. Miao, and H. Wu (2010). Sieve estimation of constant and time-varying coefficients in nonlinear ordinary differential equation models by considering both numerical error and measurement error. *The Annals of Statistics* 38, 2351–2387.
- Xun, X., J. Cao, B. Mallick, R. J. Carroll, and A. Maity (2013). Parameter estimation of partial differential equation models.

7 Appendix

7.1 Problem specific algorithms

This section provides algorithms for the extension of the probabilistic modelling of solution uncertainty to deal with the MBVP and DIFP. Algorithm 4 provides a Metropolis-Hastings implementation of the Markov chain Monte Carlo algorithm from the two state mixed boundary value problem (5) with boundary constraint $[v(a), u(b)] - [v^*(a), u^*(b)] = [0, 0]$. Since these models may be subject to solution multiplicity, Algorithm 5 provides the corresponding parallel tempering (Geyer, 1991) implementation to permit efficient exploration of the space of $u(a)$. Algorithm 6 describes forward simulation for the delay initial function problem (6). In the context of the inverse problem, Algorithm 7 describes a Metropolis-Hastings implementation of the Markov chain Monte Carlo sampler for drawing realizations from the posterior distribution of the unknowns in the JAK-STAT system problem described in Section 5.2. Algorithm 8 describes its corresponding parallel tempering implementation.

Algorithm 4 Metropolis-Hastings algorithm to draw L samples, $[u(t_1), \dots, u(t_T), v(t_1), \dots, v(t_T)]$, from the probabilistic ODE mixed boundary value problem solution model, conditional on $u^*(b), v^*(a), \theta, \Psi_N, N$ and a discretization grid $\mathbf{s} = [s_1, \dots, s_N]$

At time $s_1 = a$ Initialize the unknown boundary value $u(a) \sim \pi(\cdot)$ by sampling from the prior π ;
 Use Algorithm 1 to conditionally simulate a realization, $[u(t_1), \dots, u(t_T), v(t_1), \dots, v(t_T)]$, of the associated probabilistic ODE initial value problem solution model given $u(a), v^*(a), \theta, \Psi_N, N$ and discretization grid $\mathbf{s} = [s_1, \dots, s_N]$;

for $\ell = 1 : L$ **do**

Propose unknown boundary value $u'(a) \sim q\{\cdot | u(a)\}$ from a proposal density q ;

Use Algorithm 1 to conditionally simulate a realization, $[u'(t_1), \dots, u'(t_T), v'(t_1), \dots, v'(t_T)]$, of the associated probability model for the ODE initial value problem, conditional on $u'(a), v^*(a), \theta, \Psi_N, N$ and discretization grid $\mathbf{s} = [s_1, \dots, s_N]$;

Compute the rejection ratio,

$$\rho = \frac{q\{u(a) | u'(a)\} \pi\{u(a)\} p\{u(b) | u^*(b)\}}{q\{u'(a) | u(a)\} \pi\{u'(a)\} p\{u'(b) | u^*(b)\}};$$

if $\min\{1, \rho\} > U[0, 1]$ **then**

Update $u(a) \leftarrow u'(a)$;

Update $[u(t_1), \dots, u(t_T), v(t_1), \dots, v(t_T)] \leftarrow [u'(t_1), \dots, u'(t_T), v'(t_1), \dots, v'(t_T)]$;

end if

Return $[u(t_1), \dots, u(t_T), v(t_1), \dots, v(t_T)]$.

end for

Algorithm 5 Parallel tempering algorithm with C chains to draw L samples, $[u(t_1), \dots, u(t_T), v(t_1), \dots, v(t_T)]$, from the solution uncertainty model for the ODE mixed boundary value problem, conditional on $u^*(b), v^*(a), \theta, \Psi_N, N$ and a discretization grid $\mathbf{s} = [s_1, \dots, s_N]$

Define the probability ξ of performing a swap move between two randomly chosen chains at each iteration, and define a temperature vector $\gamma \in (0, 1]^C$, such that $\gamma_C = 1$ denoted by corresponding subscripts;

At time $s_1 = a$ Initialize the unknown boundary value $u(a)_{(1)} \sim \pi(\cdot)$ by sampling from the prior π and make $C - 1$ additional copies;

Use Algorithm 1 to conditionally simulate a sample, $[u_{(1)}(t_1), \dots, u_{(1)}(t_T), v_{(1)}(t_1), \dots, v_{(1)}(t_T)]$, from the probabilistic ODE mixed boundary value problem solution model, conditional on $u_{(1)}(a), v^*(a), \theta, \Psi_N, N$ and a discretization grid $\mathbf{s} = [s_1, \dots, s_N]$ and make $C - 1$ additional copies denoted by corresponding subscripts;

for $\ell = 1 : L$ **do**

if $\xi > U[0, 1]$ **then**

Propose a swap between $i, j \sim q(i, j)$, $1 \leq i, j \leq C, i \neq j$, where q is a proposal.

Compute the rejection ratio,

$$\rho = \frac{p \{u(b)_{(i)} \mid u^*(b)\}^{\gamma_i} p \{u(b)_{(j)} \mid u^*(b)\}^{\gamma_j}}{p \{u(b)_{(i)} \mid u^*(b)\}^{\gamma_j} p \{u(b)_{(j)} \mid u^*(b)\}^{\gamma_i}};$$

if $\min(1, \rho) > U[0, 1]$ **then**

Swap initial conditions $u(a)_{(i)}$ and $u(a)_{(j)}$;

end if

end if

for $c = 1 : C$ **do**

Perform one iteration of Metropolis-Hastings Algorithm 4, using instead a tempered likelihood to compute the rejection ratio:

$$\rho = \frac{q \{u(a)_{(c)} \mid u'(a)_{(c)}\} \pi \{u(a)_{(c)}\} p \{u(b)_{(c)} \mid u^*(b)\}^{\gamma_c}}{q \{u'(a)_{(c)} \mid u(a)_{(c)}\} \pi \{u'(a)_{(c)}\} p \{u'(b)_{(c)} \mid u^*(b)\}^{\gamma_c}},$$

with temperature γ_c ;

end for

Return $[u_{(C)}(t_1), \dots, u_{(C)}(t_T), v_{(C)}(t_1), \dots, v_{(C)}(t_T)]$.

end for

Algorithm 6 Sampling u from the probabilistic solver evaluated over the grid $\mathbf{t} = [t_1, \dots, t_T]$ for an ODE delay initial function problem, given $\phi, \tau, \theta, \Psi_N, N$ and a discretization grid $\mathbf{s} = [s_1, \dots, s_N]$

At time $s_1 = a$, sample $u^0(a - \tau) \sim \phi(a - \tau)$ and initialize the derivative $\mathbf{f}_1 = f \{s_1, u^*(a), u^0(a - \tau), \theta\}$; define m^0, m_t^0, C^0, C_t^0 as in (7);

for $n = 1 : N$ **do**

If $n = 1$, set $g_1 = C_t^0(s_1, s_1) + C_t^0(s_1 - \tau, s_1 - \tau) + 2C_t^0(s_1, s_1 - \tau)$, otherwise set $g_n = 2C_t^{n-1}(s_n, s_n) + C_t^{n-1}(s_n - \tau, s_n - \tau) + 2C_t^{n-1}(s_n, s_n - \tau)$; Compute,

$$\begin{aligned} m^n(\mathbf{s}) &= m^{n-1}(\mathbf{s}) + g_n^{-1} \int_a^{\mathbf{s}} C_t^{n-1}(z, s_n) dz \{f_n - m_t^{n-1}(s_n)\}, \\ m^n(\mathbf{s} - \tau) &= m^{n-1}(\mathbf{s} - \tau) + g_n^{-1} \int_a^{\mathbf{s} - \tau} C_t^{n-1}(z, s_n) dz \{f_n - m_t^{n-1}(s_n)\}, \\ m_t^n(\mathbf{s}) &= m_t^{n-1}(\mathbf{s}) + g_n^{-1} C_t^{n-1}(\mathbf{s}, s_n) \{f_n - m_t^{n-1}(s_n)\}, \\ C^n(\mathbf{s}, \mathbf{s}) &= C^{n-1}(\mathbf{s}, \mathbf{s}) - g_n^{-1} \int_a^{\mathbf{s}} C_t^{n-1}(z, s_n) dz \left\{ \int_a^{\mathbf{s}} C_t^{n-1}(z, s_n) dz \right\}^\top, \\ C_t^n(\mathbf{s}, \mathbf{s}) &= C_t^{n-1}(\mathbf{s}, \mathbf{s}) - g_n^{-1} C_t^{n-1}(\mathbf{s}, s_n) C_t^{n-1}(s_n, \mathbf{s}), \\ \int_a^{\mathbf{s}} C_t^n(z, \mathbf{s}) dz &= \int_a^{\mathbf{s}} C_t^{n-1}(z, \mathbf{s}) dz - g_n^{-1} \int_a^{\mathbf{s}} C_t^{n-1}(z, s_n) dz C_t^{n-1}(s_n, \mathbf{s}), \\ \int_a^{\mathbf{s} - \tau} C_t^n(z, \mathbf{s}) dz &= \int_a^{\mathbf{s} - \tau} C_t^{n-1}(z, \mathbf{s}) dz - g_n^{-1} \int_a^{\mathbf{s} - \tau} C_t^{n-1}(z, s_n) dz C_t^{n-1}(s_n, \mathbf{s}); \end{aligned}$$

if $n < N$ **then**

sample step ahead realization $u^n(s_{n+1})$ from the predictive distribution of the state,

$$p \{u(s_{n+1}) \mid f_n, \Psi_N\} = \mathcal{N} \{u(s_{n+1}) \mid m^n(s_{n+1}), C^m(s_{n+1}, s_{n+1})\};$$

if $s_{n+1} - \tau < a$ **then**

sample $u^n(s_{n+1} - \tau) \sim \phi(s_{n+1} - \tau)$,

else

sample $u^n(s_{n+1} - \tau) \sim \mathcal{N} \{m^n(s_{n+1} - \tau), C^n(s_{n+1} - \tau, s_{n+1} - \tau)\}$;

end if

and evaluate the delay differential equation model $\mathbf{f}_{n+1} = f \{s_{n+1}, u^n(s_{n+1}), u^n(s_{n+1} - \tau), \theta\}$;

end if

end for

Return $[u(t_1), \dots, u(t_T)] \sim \mathcal{GP} \{m^N(\mathbf{t}), C^N(\mathbf{t}, \mathbf{t})\}$, where $\mathbf{t} \subset \mathbf{s}$.

Algorithm 7 Metropolis-Hastings algorithm to draw L samples from the posterior distribution with density $p\{\theta, \tau, \phi, \alpha, \lambda, u(t_1), \dots, u(t_T) \mid y(t_1), \dots, y(t_T), \Sigma, N\}$ given observations on a transformation \mathcal{G} of the solution of an ODE delay initial function problem.

Initialize $\theta, \tau, \phi, \alpha, \lambda \sim \pi(\cdot)$ where π is the prior density;

Use Algorithm 6 to conditionally simulate a vector of realizations, $[u(t_1), \dots, u(t_T)]$, of the associated probabilistic ODE delay initial function problem solution model given θ, τ, ϕ, N and discretization grid $\mathbf{s} = [s_1, \dots, s_N]$;

for $\ell = 1 : L$ **do**

Propose $\theta', \tau', \phi' \sim q(\cdot \mid \theta, \tau, \phi)$ where q is a proposal density;

Use Algorithm 6 to conditionally simulate a vector of realizations, $[u'(t_1), \dots, u'(t_T)]$, of the associated probabilistic ODE delay initial function problem solution model given $\theta', \tau', \phi', \alpha, \lambda, N$ and discretization grid $\mathbf{s} = [s_1, \dots, s_N]$;

Compute the rejection ratio,

$$\rho = \frac{q(\theta, \tau, \phi \mid \theta', \tau', \phi')}{q(\theta', \tau', \phi' \mid \theta, \tau, \phi)} \frac{\pi(\theta, \tau, \phi)}{\pi(\theta', \tau', \phi')} \frac{p[y(t_1), \dots, y(t_T) \mid \mathcal{G}\{u(t_1, \theta), \theta\}, \dots, \mathcal{G}\{u(t_T, \theta), \theta\}, \Sigma]}{p[y(t_1), \dots, y(t_T) \mid \mathcal{G}\{u'(t_1, \theta'), \theta'\}, \dots, \mathcal{G}\{u'(t_T, \theta'), \theta'\}, \Sigma]};$$

if $\min(1, \rho) > \text{U}[0, 1]$ **then**

Update $[\theta, \tau, \phi] \leftarrow (\theta', \tau', \phi')$;

Update $[u(t_1, \theta), \dots, u(t_T, \theta)] \leftarrow [u'(t_1, \theta'), \dots, u'(t_T, \theta')]$;

end if

Propose $\alpha', \lambda' \sim q(\cdot \mid \alpha, \lambda)$ where q is a proposal density.

Use Algorithm 6 to conditionally simulate a vector of realizations, $[u'(t_1), \dots, u'(t_T)]$, of the associated probabilistic ODE delay initial function problem solution model given $\theta, \tau, \phi, \alpha', \lambda', N$ and discretization grid $\mathbf{s} = [s_1, \dots, s_N]$;

Compute the rejection ratio,

$$\rho = \frac{q(\alpha, \lambda \mid \alpha', \lambda')}{q(\alpha', \lambda' \mid \alpha, \lambda)} \frac{\pi(\alpha, \lambda)}{\pi(\alpha', \lambda')} \frac{p[y(t_1), \dots, y(t_T) \mid \mathcal{G}\{u(t_1, \theta), \theta\}, \dots, \mathcal{G}\{u(t_T, \theta), \theta\}, \Sigma]}{p[y(t_1), \dots, y(t_T) \mid \mathcal{G}\{u'(t_1, \theta), \theta\}, \dots, \mathcal{G}\{u'(t_T, \theta), \theta\}, \Sigma]};$$

if $\min(1, \rho) > \text{U}[0, 1]$ **then**

Update $[\alpha, \lambda] \leftarrow [\alpha', \lambda']$;

Update $[u(t_1, \theta), \dots, u(t_T, \theta)] \leftarrow [u'(t_1, \theta), \dots, u'(t_T, \theta)]$;

end if

Return $[\theta, \tau, \phi, \alpha, \lambda, u(t_1, \theta), \dots, u(t_T, \theta)]$.

end for

Algorithm 8 Parallel tempering algorithm with C chains to draw L samples from the posterior distribution with density $p(\theta, \tau, \phi, \alpha, \lambda, u(t_1), \dots, u(t_T) \mid y(t_1), \dots, y(t_T), \Sigma, N)$ given observations on a transformation \mathcal{G} of the solution of an ODE delay initial function problem with unknown parameters.

Define the probability ξ of performing a swap move between two randomly chosen chains at each iteration, and define a temperature vector $\gamma \in (0, 1]^C$, such that $\gamma_C = 1$;

Initialize $\theta_{(1)}, \tau_{(1)}, \phi_{(1)}, \alpha_{(1)}, \lambda_{(1)} \sim \pi(\cdot)$ where π is the prior density and create $C - 1$ additional copies denoting each by the corresponding subscript;

for $\ell = 1 : L$ **do**

if $\xi > U[0, 1]$ **then**

Propose a swap between $i, j \sim q(i, j)$, $1 \leq i, j \leq C, i \neq j$, where q is a proposal.

Compute the rejection ratio,

$$\rho = \frac{p[y(t_1), \dots, y(t_T) \mid \mathcal{G}\{u_{(i)}(t_1, \theta_{(i)}), \theta_{(i)}\}, \dots, \mathcal{G}\{u_{(i)}(t_T, \theta_{(i)}), \theta_{(i)}\}, \Sigma]^{\gamma_i}}{p[y(t_1), \dots, y(t_T) \mid \mathcal{G}\{u_{(j)}(t_1, \theta_{(j)}), \theta_{(j)}\}, \dots, \mathcal{G}\{u_{(j)}(t_T, \theta_{(j)}), \theta_{(j)}\}, \Sigma]^{\gamma_j}} \cdot \frac{p[y(t_1), \dots, y(t_T) \mid \mathcal{G}\{u_{(j)}(t_1, \theta_{(j)}), \theta_{(j)}\}, \dots, \mathcal{G}\{u_{(j)}(t_T, \theta_{(j)}), \theta_{(j)}\}, \Sigma]^{\gamma_j}}{p[y(t_1), \dots, y(t_T) \mid \mathcal{G}\{u_{(i)}(t_1, \theta_{(i)}), \theta_{(i)}\}, \dots, \mathcal{G}\{u_{(i)}(t_T, \theta_{(i)}), \theta_{(i)}\}, \Sigma]^{\gamma_i}};$$

if $\min(1, \rho) > U[0, 1]$ **then**

Swap parameter vectors $[\theta_{(i)}, \tau_{(i)}, \phi_{(i)}, \alpha_{(i)}, \lambda_{(i)}] \leftrightarrow [\theta_{(j)}, \tau_{(j)}, \phi_{(j)}, \alpha_{(j)}, \lambda_{(j)}]$;

end if

end if

for $c = 1 : C$ **do**

Perform one iteration of Metropolis-Hastings Algorithm 7, using instead a tempered likelihood to compute the rejection ratios:

$$\rho = \frac{q(\theta_{(c)}, \tau_{(c)}, \phi_{(c)} \mid \theta'_{(c)}, \tau'_{(c)}, \phi'_{(c)}) \pi(\theta_{(c)}, \tau_{(c)}, \phi_{(c)})}{q(\theta'_{(c)}, \tau'_{(c)}, \phi'_{(c)} \mid \theta_{(c)}, \tau_{(c)}, \phi_{(c)}) \pi(\theta'_{(c)}, \tau'_{(c)}, \phi'_{(c)})} \cdot \frac{p[y(t_1), \dots, y(t_T) \mid \mathcal{G}\{u_{(c)}(t_1, \theta_{(c)}), \theta_{(c)}\}, \dots, \mathcal{G}\{u_{(c)}(t_T, \theta_{(c)}), \theta_{(c)}\}, \Sigma]^{\gamma_c}}{p[y(t_1), \dots, y(t_T) \mid \mathcal{G}\{u'_{(c)}(t_1, \theta'_{(c)}), \theta'_{(c)}\}, \dots, \mathcal{G}\{u'_{(c)}(t_T, \theta'_{(c)}), \theta'_{(c)}\}, \Sigma]^{\gamma_c}},$$

and,

$$\rho = \frac{q(\alpha_{(c)}, \lambda_{(c)} \mid \alpha'_{(c)}, \lambda'_{(c)}) \pi(\alpha_{(c)}, \lambda_{(c)})}{q(\alpha'_{(c)}, \lambda'_{(c)} \mid \alpha_{(c)}, \lambda_{(c)}) \pi(\alpha'_{(c)}, \lambda'_{(c)})} \cdot \frac{p[y(t_1), \dots, y(t_T) \mid \mathcal{G}\{u_{(c)}(t_1, \theta_{(c)}), \theta_{(c)}\}, \dots, \mathcal{G}\{u_{(c)}(t_T, \theta_{(c)}), \theta_{(c)}\}, \Sigma]^{\gamma_c}}{p[y(t_1), \dots, y(t_T) \mid \mathcal{G}\{u'_{(c)}(t_1, \theta_{(c)}), \theta_{(c)}\}, \dots, \mathcal{G}\{u'_{(c)}(t_T, \theta_{(c)}), \theta_{(c)}\}, \Sigma]^{\gamma_c}},$$

with temperature γ_c ;

end for

Return $[\theta_{(C)}, \tau_{(C)}, \phi_{(C)}, \alpha_{(C)}, \lambda_{(C)}, u_{(C)}(t_1, \theta_{(C)}), \dots, u_{(C)}(t_T, \theta_{(C)})]$.

end for

7.2 Probabilistic solution as latent function estimation

We take a process convolution view of the model presented in Section 3. Let $\mathcal{F} = L^2(\mathbb{R}; (H, \mathcal{A}, \mu^0))$ be the space of square-integrable random functions and \mathcal{F}^* be its dual space of linear functionals. The solution and its derivative will be modelled by an integral transform using the linear continuous operators R and Q defining a mapping from \mathcal{F} to \mathcal{F}^* . The associated kernels are the deterministic, square-integrable function $R_\lambda : \mathbb{R} \times \mathbb{R} \rightarrow \mathbb{R}$ and its integrated version $Q_\lambda(t_j, t_k) = \int_a^{t_k} R_\lambda(z, t_k) dz$. The operators $R, Q, R^\dagger, Q^\dagger$ are defined, for $u \in \mathcal{F}$ and $v \in \mathcal{F}^*$, as $Ru(t) = \int R_\lambda(t, z)u(z)dz$ and $Qu(t) = \int Q_\lambda(t, z)u(z)dz$, with adjoints $R^\dagger v(t) = \int R_\lambda(z, t)v(z)dz$ and $Q^\dagger v(t) = \int Q_\lambda(z, t)v(z)dz$ respectively.

Estimating the solution of a differential equation model may be restated as a problem of inferring an underlying latent process $\zeta \in \mathcal{F}$ from noisy realizations. We consider the white noise process, $\zeta \sim \mathcal{N}(0, K)$, with covariance $K(t_j, t_k) = \alpha^{-1} \delta_{t_j}(t_k)$. We model the derivative of the solution as the integral transform,

$$u_t(t_j) = m_t^n(t_j) + R\zeta(t_j), \quad t_j \in [a, b], \quad 0 \leq n \leq N. \quad (23)$$

The differential equation solution model at time $t_j \leq b$ is then obtained by integrating the derivative u_t with respect to time over the interval $[a, t_j]$ as follows,

$$u(t_j) = \int_a^{t_j} u_t(z) dz = m^n(t_j) + Q\zeta(t_j), \quad t_j \in [a, b], \quad 0 \leq n \leq N. \quad (24)$$

Our goal is to update the prior μ^{n-1} given a new noisy derivative realizations, f_n , to obtain the probabilistic update μ^n , $1 \leq n \leq N$.

Lemma 7.1 (Updating). *The probabilistic solution $\{u^n(t), t \in [a, b]\}$ and its time derivative $\{u_t^n(t), t \in [a, b]\}$ are well-defined and distributed according to Gaussian probability measure μ^n with marginal mean functions, covariance and cross-covariance operators given by,*

$$\begin{aligned} m^n(t_j) &= m^{n-1}(t_j) + g_n^{-1} \{f_n - m_t^{n-1}(s_n)\} \int_a^{t_j} C_t^{n-1}(z, s_n) dz, \\ m_t^n(t_j) &= m_t^{n-1}(t_j) + g_n^{-1} \{f_n - m_t^{n-1}(s_n)\} C_t^{n-1}(t_j, s_n), \\ C^n(t_j, t_k) &= C^{n-1}(t_j, t_k) - g_n^{-1} \int_a^{t_j} C_t^{n-1}(z, s_n) dz \int_a^{t_k} C_t^{n-1}(s_n, z) dz, \\ C_t^n(t_j, t_k) &= C_t^{n-1}(t_j, t_k) - g_n^{-1} C_t^{n-1}(t_j, s_n) C_t^{n-1}(s_n, t_k), \\ \int_a^{t_j} C_t^n(z, t_k) dz &= \int_a^{t_j} C_t^{n-1}(z, t_k) dz - g_n^{-1} \int_a^{t_j} C_t^{n-1}(z, s_n) dz C_t^{n-1}(s_n, t_k), \\ \int_a^{t_k} C_t^n(t_j, z) dz &= \left\{ \int_a^{t_k} C_t^n(z, t_j) dz \right\}^\top \end{aligned}$$

where we define,

$$g_n := \begin{cases} C_t^0(s_1, s_1) & \text{if } n = 1, \\ 2C_t^{n-1}(s_n, s_n) & \text{if } n > 1, \end{cases}$$

and where m^0 and m_t^0 are the prior means and C^0 and C_t^0 the prior covariances of the state and derivatives defined in Section 2.

Proof. We are interested in the conditional distribution of the state $u(t) - m^{n-1}(t) \in \mathcal{F}^*$ and time derivative $u_t(t) - m_t^{n-1}(t) \in \mathcal{F}^*$ given a new noisy derivative evaluation on a mesh vertex $s_n \in [a, b]$ under the Gaussian error model,

$$f_n - m_t^{n-1}(s_n) = R\zeta(s_n) + \eta(s_n),$$

where $\eta(s_n) \sim \mathcal{N}(0, \gamma_n)$.

Construct the vector

$$[u_t - m_t^{n-1}, f_n - m_t^{n-1}(s_n)] = [R\zeta, R\zeta(s_n) + \eta(s_n)] \in \mathcal{F}^* \oplus \mathbb{R},$$

where the first element is function-valued and the second element is a scalar. This vector is jointly Gaussian with mean $M = (0, 0)$ and covariance operator C with positive definite cross-covariance operators,

$$\begin{aligned} C_{11} &= RKR^\dagger & C_{12} &= RKR^\dagger \\ C_{21} &= RKR^\dagger & C_{22} &= RKR^\dagger + \gamma_n. \end{aligned} \quad (25)$$

Since both \mathcal{F}^* and \mathbb{R} are separable Hilbert spaces, it follows from Theorem 6.20 in Stuart (2010) that the random variable $[u_t - m_t^{n-1} \mid f_n - m_t^{n-1}(s_n)]$ is well-defined and distributed according to a Gaussian probability measure with mean and covariance,

$$\begin{aligned} \mathbb{E} [u_t - m_t^{n-1} \mid f_n - m_t^{n-1}(s_n)] &= C_{12}C_{22}^{-1}(f_n - m_t^{n-1}(s_n)), \\ \text{Cov} [u_t - m_t^{n-1} \mid f_n - m_t^{n-1}(s_n)] &= C_{11} - C_{12}C_{22}^{-1}C_{21}. \end{aligned}$$

Similarly, we consider the vector $[u - m^{n-1}, f_n - m_t^{n-1}(s_n)] = [Q\zeta, R\zeta(s_n) + \eta(s_n)] \in \mathcal{F}^* \oplus \mathbb{R}$, with mean $M = (0, 0)$ and cross-covariances,

$$\begin{aligned} C_{11} &= QKQ^\dagger & C_{12} &= QKR^\dagger \\ C_{21} &= RKQ^\dagger & C_{22} &= RKR^\dagger + \gamma_n. \end{aligned}$$

By Theorem 6.20 (Stuart, 2010), the random variable $[u - m^{n-1} \mid f_n - m_t^{n-1}(s_n)]$ is well-defined and distributed according to a Gaussian probability measure with mean and covariance,

$$\begin{aligned} \mathbb{E} [u - m^{n-1} \mid f_n - m_t^{n-1}(s_n)] &= C_{12}C_{22}^{-1}(f_n - m_t^{n-1}(s_n)), \\ \text{Cov} [u - m^{n-1} \mid f_n - m_t^{n-1}(s_n)] &= C_{11} - C_{12}C_{22}^{-1}C_{21}. \end{aligned}$$

Cross-covariances are found analogously. □

A necessary condition for a well-defined probabilistic discretization model is that the cross-covariance operators, (25), between the derivative and n derivative model realizations, be positive definite. We note that this condition is satisfied by kernels R_λ that are not everywhere zero.

7.3 Proof of Theorem 3.1

Denote the exact solution satisfying (3) by $u^*(t)$. For clarity of exposition, we assume that $u(a) = 0$ and let $m^0(t) = 0$ for $t \in [a, b]$. We define $h = \max_{n=2, \dots, N} (s_n - s_{n-1})$ to be the maximum step length between subsequent discretization grid points. We would like to show that the probabilistic posterior $\{u^N(t), t \in [a, b]\}$ obtained via Algorithm 1 converges in L^1 to $u^*(t)$ as $h \rightarrow 0$ and $\lambda, \alpha^{-1} = O(h)$, concentrating at a rate proportional to h .

For a given $t \in [a, b]$ we find n such that $t \in [s_n, s_{n+1}]$, and bound the expected absolute difference between the n th probabilistic solution and the exact solution as follows,

$$\begin{aligned} \beta_n(t) &= \mathbb{E} \left\{ |u(t) - u^*(t)| \mid \mathbf{f}_{1:n}, \theta, \Psi_N \right\} \\ &= \mathbb{E} \left[u(t) - u^*(t) \mid \mathbf{f}_{1:n}, \theta, \Psi_N \right] \left\{ 1 - 2\Phi \left(-\frac{\mathbb{E}[u(t) - u^*(t) \mid \mathbf{f}_{1:n}, \theta, \Psi_N]}{\sqrt{C^n(t, t)}} \right) \right\} \\ &\quad + \sqrt{\frac{2}{\pi} C^n(t, t)} \exp \left\{ -\frac{(\mathbb{E}[u(t) - u^*(t) \mid \mathbf{f}_{1:n}, \theta, \Psi_N])^2}{2C^n(t, t)} \right\}, \\ &\leq \left| \mathbb{E} \{ u(t) - u^*(t) \mid \mathbf{f}_{1:n}, \theta, \Psi_N \} \right| + \sqrt{2C^1(t, t)} \end{aligned} \tag{26}$$

where Φ is the cdf of the standard normal distribution. The second equality uses the fact that the argument is normally distributed, so that its absolute value follows a folded normal distribution (see, for example, Leone et al., 1961). The inequality $C^n(t, t) \leq C^1(t, t)$ follows from Lemma 7.2.

Next we want to bound the first term of (26). For $1 \leq n < N$, the n th step probabilistic solution is a Gaussian process that is mean-square differentiable on $[a, b]$. Therefore we can write the difference between the expected probabilistic solution and the exact solution, using a Taylor expansions around s_n ,

$$\begin{aligned} &\mathbb{E} [u(t) - u^*(t) \mid \mathbf{f}_{1:n}, \theta, \Psi_N] \\ &= \mathbb{E} [u(s_n) - u^*(s_n) \mid \mathbf{f}_{1:n}, \theta, \Psi_N] + (t - s_n) \mathbb{E} [u_t(s_n) - f \{s_n, u^*(s_n), \theta\} \mid \mathbf{f}_{1:n}, \theta, \Psi_N] + O(h^2) \end{aligned}$$

Next we use the Bayesian updating result from Lemma 7.1 to rewrite the probabilistic solution at step n in terms of the probabilistic solution at step $(n-1)$ and the step ahead derivative realization $f \{s_n, u^{n-1}(s_n), \theta\}$,

and then rearrange the terms, as follows,

$$\begin{aligned}
& \mathbb{E}[u(t) - u^*(t) \mid \mathbf{f}_{1:n}, \theta, \Psi_N] \\
&= \mathbb{E}[u(s_n) - u^*(s_n) \mid \mathbf{f}_{1:n-1}, \theta, \Psi_N] + \frac{C^{n-1}(s_n, s_n)}{C_t^{n-1}(s_n, s_n)} \mathbb{E}[\{f\{s_n, u^{n-1}(s_n), \theta\} - u_t(s_n)\} \mid \mathbf{f}_{1:n-1}, \theta, \Psi_N] \\
&\quad + (t - s_n) \mathbb{E}[f\{s_n, u^{n-1}(s_n), \theta\} - f\{s_n, u^*(s_n), \theta\} \mid \mathbf{f}_{1:n-1}, \theta, \Psi_N] + O(h^2).
\end{aligned} \tag{27}$$

Now, we can bound our expected difference between the probabilistic and exact solutions by using (26), (27), and Jensen's inequality:

$$\begin{aligned}
\beta_n(t) &\leq \beta_{n-1}(s_n) + |t - s_n| \cdot \mathbb{E}\{|f\{s_n, u^{n-1}(s_n), \theta\} - f\{s_n, u^*(s_n), \theta\}\} \mid \mathbf{f}_{1:n-1}, \theta, \Psi_N\} \\
&\quad + \frac{C^{n-1}(s_n, s_n)}{C_t^{n-1}(s_n, s_n)} \mathbb{E}\{|f\{s_n, u^{n-1}(s_n), \theta\} - u_t(s_n)\} \mid \mathbf{f}_{1:n-1}, \theta, \Psi_N\} + \sqrt{2C^1(t, t)} + O(h^2).
\end{aligned}$$

The Lipschitz continuity of f and boundedness of $\mathbb{E}\{|f\{s_n, u^{n-1}(s_n), \theta\} - u_t(s_n)\} \mid \mathbf{f}_{1:n-1}, \theta, \Psi_N\}$ (by Lipschitz continuity of f and recursive definition of the posterior mean) then implies:

$$\begin{aligned}
\beta_n(t) &\leq \beta_{n-1}(s_n) + L|t - s_n|\beta_{n-1}(s_n) + O\left(\frac{C^{n-1}(s_n, s_n)}{C_t^{n-1}(s_n, s_n)}\right) + O(\sqrt{C^1(t, t)}) + O(h^2) \quad ll \\
&= \beta_{n-1}(s_n) (1 + L|t - s_n|) + O(h^2).
\end{aligned}$$

It can be shown (see, for example, Butcher, 2008, p.67-68) that the following inequality holds:

$$\beta_n(t) \leq \begin{cases} \beta_0(s_1) + hB(t - a), & L = 0, \\ \exp\{(t - a)L\}\beta_0(s_1) + \exp\{(t - a)L - 1\}hB/L, & L > 0, \end{cases}$$

where B is the constant upper bound on all the remainders. This expression tends to 0 as $\alpha^{-1}, \lambda, h \rightarrow 0$, since $\beta_0(s_1) = 0$. Then, taking the expectation of $\beta_n(t)$ with respect to the vector of model evaluations, we obtain the expectation,

$$\mathbb{E}\{|u(t) - u^*(t)| \mid \theta, \Psi_N\} = O(h), \quad \text{as } \alpha^{-1}, \lambda \rightarrow 0.$$

Therefore the probabilistic solution $[u(t) \mid \theta, \Psi_N]$ converges in L^1 to $u^*(t)$ at least as fast as $O(h)$.

Note that the assumption that auxiliary parameters, λ and α^{-1} , associated with the solver tend to zero with the step size is analogous to maintaining a constant number of steps in a k -step numerical method regardless of the step size.

7.4 Properties of the covariance

In this section we present some results regarding covariance structures that are used in the proof of Theorem 3.1.

Lemma 7.2. *For $1 < n \leq N$ and $t \in [a, b]$, the variances for the state and derivative obtained sequentially via Algorithm 1 satisfy:*

$$\begin{aligned}
C^n(t, t) &\leq C^1(t, t), \\
C_t^n(t, t) &\leq C_t^1(t, t).
\end{aligned}$$

Proof. We use the fact that $C_t^n(t, t) \geq 0$ for all n and the recurrence from Lemma 7.1, we obtain:

$$\begin{aligned}
C_t^n(t, t) &= C_t^{n-1}(t, t) - g_n^{-1} C_t^{n-1}(t, s_n) C_t^{n-1}(s_n, t), \\
&\leq C_t^{n-1}(t, t) \leq \dots \leq C_t^1(t, t).
\end{aligned}$$

Similarly,

$$\begin{aligned}
C^n(t, t) &= C^{n-1}(t, t) - g_n^{-1} \int_a^t C_t^{n-1}(z, s_n) dz \int_a^t C_t^{n-1}(s_n, z) dz, \\
&\leq C^{n-1}(t, t) \leq \dots \leq C^1(t, t).
\end{aligned}$$

□

Lemma 7.3. *The covariances, $C^n(t_j, t_k)$ and $C_t^n(t_j, t_k)$, obtained at each step of Algorithm 1 tend to zero at the rate $O(h^4)$, as $h \rightarrow 0$ and $\lambda, \alpha^{-1} = O(h)$ if the covariance function R_λ is stationary and satisfies:*

$$RR(t, t) - \frac{RR(t+d, t)RR(t+d, t)}{RR(t, t)} = O(h^4), \quad \lambda, \alpha^{-1} = O(h), \quad h \rightarrow 0, \quad (28)$$

$$QQ(t, t) - \frac{QR(t+d, t)QR^\dagger(t+d, t)}{RR(t, t)} = O(h^4), \quad \lambda, \alpha^{-1} = O(h), \quad h \rightarrow 0, \quad (29)$$

where $d > 0$, $t, t+d \in [a, b]$, and $\lambda \geq h$.

Proof. From Lemma 7.2 and assumption (28) we obtain,

$$C_t^n(t, t) \leq C_t^1(t, t) = RR(t, t) - \frac{RR(t, s_1)RR(s_1, t)}{RR(s_1, s_1)} = O(h^4), \quad \lambda, \alpha^{-1} = O(h), \quad h \rightarrow 0, \quad t \in [a, b], \quad 1 \leq n \leq N.$$

Similarly, using Lemma 7.2 and assumption (29) yields,

$$C^n(t, t) \leq C^1(t, t) = QQ(t, t) - \frac{QR(t, s_1)QR^\dagger(t, s_1)}{RR(s_1, s_1)} = O(h^4), \quad \lambda, \alpha^{-1} = O(h), \quad h \rightarrow 0, \quad t \in [a, b], \quad 1 \leq n \leq N.$$

Then, by the Cauchy-Schwarz inequality,

$$|C_t^n(t_j, t_k)|, |C^n(t_j, t_k)| = O(h^4), \quad \lambda, \alpha^{-1} = O(h), \quad h \rightarrow 0, \quad t_j, t_k \in [a, b], \quad 1 \leq n \leq N. \quad \square$$

It is straightforward to show that the square exponential and uniform covariance functions considered in this paper are stationary and symmetric and satisfy conditions (28) and (29).

Lemma 7.4. *The model-prior mismatch, $C_t^{n-1}(s_n, s_n)$, $1 \leq n \leq N$ obtained under for Algorithm 1, tends to zero at the rate $O(h^4)$ as $N \rightarrow \infty$ in such a way that $h \rightarrow 0$ when conditions (28) and (29) are satisfied.*

Proof. The proof follows immediately from Lemma 7.3. □

7.5 Some covariance kernels and their convolutions

Choice of the covariance function is related to the assumed smoothness of the exact but unknown solution. The examples in this paper utilise two types of covariance functions, although the results are more generally applicable. It is important to be aware that imposing unrealistically strict smoothness assumptions on the state space by choice of covariance structure may introduce estimation bias if the exact solution is not at least as smooth. Therefore, in cases where the solution smoothness is not known a priori, one can err on the side of caution by using less regular kernels. In this paper we chose to work with stationary derivative covariance structures for simplicity, however there will be classes of problems where non-stationary kernels may be more appropriate.

Let $w = \frac{1}{2\lambda}$. The squared exponential covariance, obtained by convolving the kernel,

$$R_\lambda(t_j, t_k) = \exp \left\{ -\frac{2(t_j - t_k)^2}{w^2} \right\},$$

is infinitely differentiable. Thus, we utilise this covariance structure in the solution of the Lorenz63 model, the Navier-Stokes equations, the Lane-Emden mixed boundary value problem, and the heat equation. Given the scale of the squared exponential kernel, we suggest choosing the length-scale, λ , to be at least twice as large as the maximum distance between subsequent discretization grid points. This choice places most of the mass of the derivative covariance between the predictive location and the location of the last model evaluation obtained.

In contrast, solutions for systems of delay initial function problems are often characterized by second derivative discontinuities at the lag locations. In order to avoid bias from over-smoothing, we utilise the uniform covariance structure for modelling the derivative. This covariance, obtained by convolving the kernel,

$$R_\lambda(t_j, t_k) = 1_{(t_j - \lambda, t_j + \lambda)}(t_k),$$

is non-differentiable. Given the scale of the uniform kernel, choosing the length-scale λ , to be exactly half of the step length ensures that the resulting step ahead prediction captures information from exactly one previous model evaluation. A length-scale greater than half the step size provides estimates that are analogous to a multi-step numerical solver.

Closed form expressions for the pairwise convolutions for the two covariance functions are provided below. Let R_λ be the squared exponential kernel and let Q_λ be its integrated version. Then,

$$\begin{aligned}\alpha RR(t_j, t_k) &= \sqrt{\pi}\lambda \exp\left\{-\frac{(t_j-t_k)^2}{w^2}\right\}; \\ \alpha QR(t_j, t_k) &= \pi\lambda^2 \left[\operatorname{erf}\left\{\frac{t_j-t_k}{w}\right\} + \operatorname{erf}\left\{\frac{t_k-a}{w}\right\}\right]; \\ \alpha QQ(t_j, t_k) &= \pi\lambda^2 \left[(t_j-a)\operatorname{erf}\left\{\frac{t_j-a}{w}\right\} - (t_k-t_j)\operatorname{erf}\left\{\frac{t_k-t_j}{w}\right\} + (t_k-a)\operatorname{erf}\left\{\frac{t_k-a}{w}\right\}\right]; \\ &\quad + 2\sqrt{\pi}\lambda^3 \left[\exp\left\{-\frac{(t_j-a)^2}{w^2}\right\} - \exp\left\{-\frac{(t_k-t_j)^2}{w^2}\right\} + \exp\left\{-\frac{(t_k-a)^2}{w^2}\right\} - 1\right].\end{aligned}$$

Next, let R_λ be the uniform kernel and let Q_λ be its integrated version. Then,

$$\begin{aligned}\alpha RR(t_j, t_k) &= \{\min(t_j, t_k) - \max(t_j, t_k) + 2\lambda\} 1_{\mathbb{R}^+}\{\min(t_j, t_k) - \max(t_j, t_k) + 2\lambda\}; \\ \alpha QR(t_j, t_k) &= 2\lambda\{\min(t_j - \lambda, t_k + \lambda) - \max(a + \lambda, t_k - \lambda)\} 1_{\mathbb{R}^+}\{\min(t_j - \lambda, t_k + \lambda) - \max(a + \lambda, t_k - \lambda)\} \\ &\quad + (t_j - a)\{\max(t_j, t_k) - a - 2\lambda\} 1_{\mathbb{R}^+}\{\max(t_j, t_k) - a - 2\lambda\}, \\ &\quad + [(t_j + \lambda)\{\min(t_j, t_k) - \max(a + \lambda, t_j - \lambda, t_k - \lambda) + \lambda\} \\ &\quad \quad - \frac{1}{2}\{\min(t_j, t_k) - \max(a + \lambda, t_j - \lambda, t_k - \lambda) + \lambda\}^2] 1_{\mathbb{R}^+}\{\min(t_j, t_k) + \lambda - \max(a + \lambda, t_j - \lambda, t_k - \lambda)\} \\ &\quad + [(\lambda - a)\{\min(a + \lambda, t_j - \lambda, t_k + \lambda) - (t_k - \lambda)\} \\ &\quad \quad + \frac{1}{2}\{\min(a + \lambda, t_j - \lambda, t_k + \lambda) - (t_k - \lambda)\}^2] 1_{\mathbb{R}^+}\{\min(a + \lambda, t_j - \lambda, t_k + \lambda) - (t_k - \lambda)\}; \\ \alpha QQ(t_j, t_k) &= 4\lambda^2\{\min(t_j, t_k) - a - 2\lambda\} 1_{\mathbb{R}^+}\{\min(t_j, t_k) - a - 2\lambda\} \\ &\quad + 2\lambda[(t_k + \lambda)\{\min(t_j - \lambda, t_k + \lambda) - \max(a + \lambda, t_k - \lambda)\} \\ &\quad \quad - \frac{1}{2}\{\min(t_j - \lambda, t_k + \lambda) - \max(a + \lambda, t_k - \lambda)\}^2] 1_{\mathbb{R}^+}\{\min(t_j - \lambda, t_k + \lambda) - \max(a + \lambda, t_k - \lambda)\} \\ &\quad + [\frac{1}{3}\{\min(a + \lambda, t_j - \lambda, t_k - \lambda) - (a - \lambda)\}^3 + (\lambda - a)\{\min(a + \lambda, t_j - \lambda, t_k - \lambda) - (a - \lambda)\}^2 \\ &\quad \quad + (\lambda - a)^2\{\min(a + \lambda, t_j - \lambda, t_k - \lambda) - (a - \lambda)\}] 1_{\mathbb{R}^+}\{\min(a + \lambda, t_j - \lambda, t_k - \lambda) - (a - \lambda)\} \\ &\quad + (t_j - a) [\frac{1}{2}\{\min(a + \lambda, t_k - \lambda) - (t_j - \lambda)\}^2 \\ &\quad \quad + (\lambda - a)\{\min(a + \lambda, t_k - \lambda) - (t_j - \lambda)\}] 1_{\mathbb{R}^+}\{\min(a + \lambda, t_k - \lambda) - (t_j - \lambda)\} \\ &\quad + (t_k - a) [\frac{1}{2}\{\min(a + \lambda, t_j - \lambda) - (t_k - \lambda)\}^2 \\ &\quad \quad + (\lambda - a)\{\min(a + \lambda, t_j - \lambda) - (t_k - \lambda)\}] 1_{\mathbb{R}^+}\{\min(a + \lambda, t_j - \lambda) - (t_k - \lambda)\} \\ &\quad + 2\lambda[(t_j + \lambda)\{\min(t_j + \lambda, t_k - \lambda) - \max(a + \lambda, t_j - \lambda)\} \\ &\quad \quad - \frac{1}{2}\{\min(t_j + \lambda, t_k - \lambda) - \max(a + \lambda, t_j - \lambda)\}^2] 1_{\mathbb{R}^+}\{\min(t_j + \lambda, t_k - \lambda) - \max(a + \lambda, t_j - \lambda)\} \\ &\quad + [(t_j + \lambda)(t_k + \lambda)\{\min(t_j, t_k) + \lambda - \max(a + \lambda, t_j - \lambda, t_k - \lambda)\} \\ &\quad \quad - \frac{1}{2}(t_j + t_k + 2\lambda)\{\min(t_j, t_k) + \lambda - \max(a + \lambda, t_j - \lambda, t_k - \lambda)\}^2 \\ &\quad \quad + \frac{1}{3}\{\min(t_j, t_k) + \lambda - \max(a + \lambda, t_j - \lambda, t_k - \lambda)\}^3] 1_{\mathbb{R}^+}\{\min(t_j, t_k) + \lambda - \max(a + \lambda, t_j - \lambda, t_k - \lambda)\} \\ &\quad + (t_j - a)(t_k - a)\{a + 2\lambda - \max(t_j, t_k)\} 1_{\mathbb{R}^+}\{a + 2\lambda - \max(t_j, t_k)\},\end{aligned}$$

where,

$$1_A(x) = \begin{cases} 1 & \text{if } x \in A; \\ 0 & \text{otherwise.} \end{cases}$$